Computational Modeling of Environmental Co-exposure of the Oil-Derived Hydrocarbon Overload using *Pseudomonas putida* Protein (*TodX*) with Graphene Nanostructures

Patrícia Viera de Oliveira[a, *], Luiza Goulart[a], Cláudia Lange dos Santos[a], Jussane Rossato[a], M. Natália D. S. Cordeiro[b], Juan M. Ruso[c], Solange Binotto Fagan[a, *], Ivana Zanella[a], Michael González-Durruthy[b,c,*]

[a]Nanoscience Department, Universidade Franciscana, 97010-032 Rio Grande do Sul-RS, Brazil.

[b]LAQV-REQUINTE of Chemistry and Biochemistry, Faculty of Sciences, University of Porto, 4169-007 Porto, Portugal.

[c]Soft Matter and Molecular Biophysics Group, Department of Applied Physics, University of Santiago de Compostela, 15782 Santiago de Compostela, Spain.

*** To whom correspondence should be addressed**:
Patrícia Viera de Oliveira, Email: patiolivera@yahoo.com.br, Fax: (48) 3721 9687
M. González-Durruthy, Email: michael.durruthy@fc.up.pt, Fax: +351220402659
Solange Binotto Fagan, Email: solange.fagan@gmail.com, Fax: 55-32226484

'For TOC only'

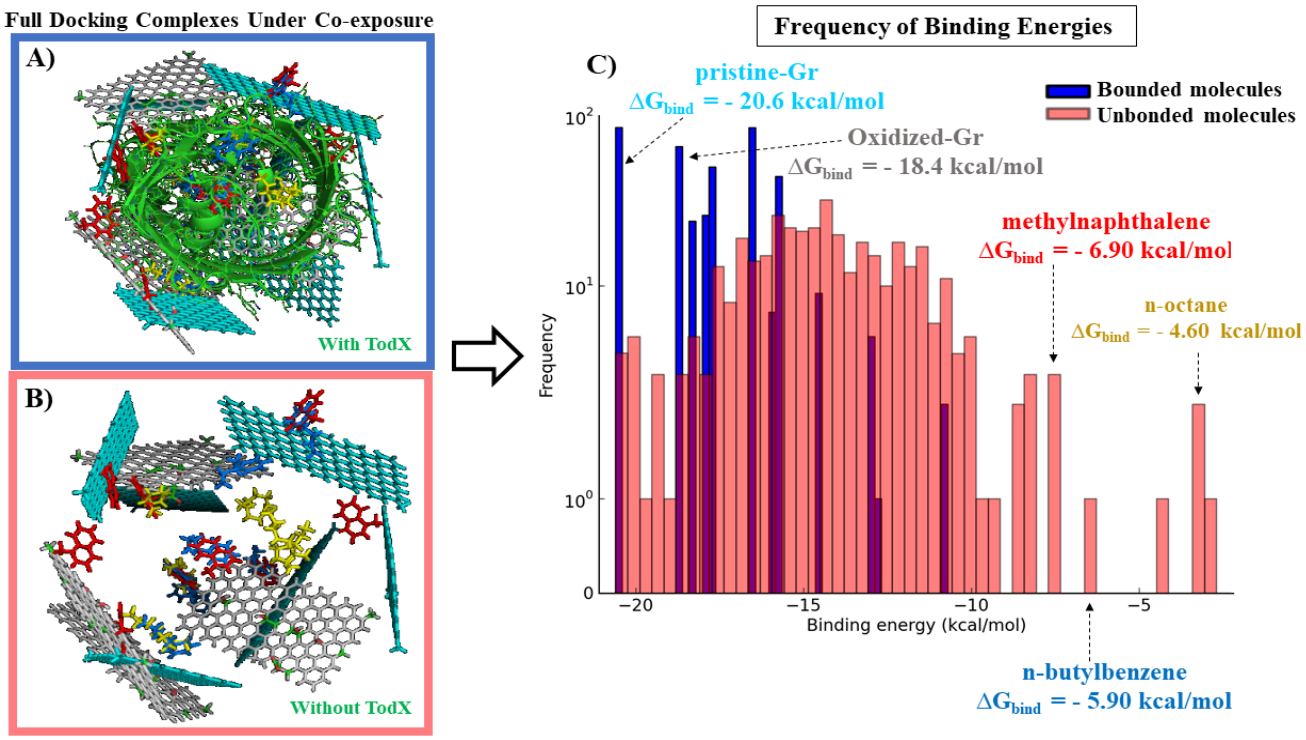
Full Docking Complexes Under Co-exposure
A)
With TodX
B)
Without TodX
Frequency of Binding Energies
C)
pristine-Gr
ΔG_bind = - 20.6 kcal/mol
Oxidized-Gr
ΔG_bind = - 18.4 kcal/mol
methylnaphthalene
ΔG_bind = - 6.90 kcal/mol
n-octane
ΔG_bind = - 4.60 kcal/mol
n-butylbenzene
ΔG_bind = - 5.90 kcal/mol
Bounded molecules
Unbonded molecules
Frequency
Binding energy (kcal/mol)

Abstract

Bioremediation is a biotechnology field that uses living organisms to remove contaminants from soil and water; therefore, they could be used to treat oil spill from the environment. Herein, we present a new mechanistic approaches combining Molecular Docking Simulation and Density Functional Theory to modeling the interactions of a heterogeneous mixture of oil-derived hydrocarbons with the *Pseudomonas putida* transporter and pristine and oxidized graphene. The theoretical evidence pointing that the binding interactions are mainly based in non-covalent bonds characteristic of physical adsorption mechanism. These results open new horizons to improve bioremediation strategies in over-saturation conditions against oil-spills and expanding the use of nanotechnologies in the context of environmental modeling health and safety.

Keywords: Oil-derived hydrocarbons, TodX protein, graphene, molecular docking, DFT-simulation

Introduction

One of the largest oil-spills in the human history was recorded in 2010 in the Gulf of Mexico on the Deepwater Horizon platform, where approximately 800 million liters of oil were spilled into the sea.[1] This environmental catastrophe caused severe impacts over the health of birds, fish, and marine mammals with a high-mortality rate in this ecosystem, including human health where the prevalence of neurological disorders and other environmental diseases currently persist.[2,3] In the present study, we tackle the environmental modeling based on the use of detoxifying microorganisms (*Pseudomonas putida*) which present efficient biochemical mechanisms to selectively-reduce the oil-derived hydrocarbons concentrations. The *Pseudomonas putida* is a bacterium which has been studied for many environmental researchers, due to its potential application in the bioremediation field. *Pseudomonas putida* is naturally adapted to actions against crude oil spillage in the environment.[4] Particularly, the outer membrane transport protein (TodX) family from *Pseudomonas putida* includes several proteins that are involved in the efficient degradation of aromatic hydrocarbons.[5-7] The biochemical function of the TodX protein allows the hydrocarbons detoxification and passage through the cell membranes.

However, the TodX hydrophobic-transport activity could be compromised in overload conditions of several pollutants.[5-7] Previous studies performed by Belchik and colaborators[8], support that a similar protein-like TcpY facilitates the transport of polychlorophenols across the outer membrane of gram-negative bacterium,[8] and likewise COG4313 proteins are possible outer membrane transporters of hydrophobic aromatic compounds.[8] Besides, Van Den Berg[9] investigated the FadL family channels, as carrier of hydrophobic molecules that work according to a lateral diffusion mechanism that contribute to the detoxification of hydrophobic aromatic compounds.

By the other hand, interesting work performed by Hearn et al.[10] tackle the structural study of the two layers of the outer membranes using *Pseudomonas putida* (TodX) and *Ralstonia pickettii* (TbuX) to address the transport mechanism of hydrocarbons using *in vitro* assays, suggesting that hydrocarbons transport mechanism is mainly based on hydrophobic transport from the extracellular environment to the periplasm through a channel hatching domain of the TodX.[10] Besides, high-performance liquid chromatography measurements strongly suggest that this microorganism *Pseudomonas putida (*TodX*)* may be useful in the biodegradation of polycyclic aromatic hydrocarbons PAHs in petrochemicals.[10,11] Following this idea, carbon nanomaterials like graphene nanostructures (pristine-Gr and oxidized-Gr) could provide new alternatives for environmental bioremediation when combined with detoxifying microorganisms (TodX protein from *Pseudomonas putida*), due to the high surface reactive ability to adsorb aromatic hydrocarbons compounds.[11-14] The pristine-Gr structures present a significantly high-affinity by aromatic hydrocarbons compounds due to the occurrence of hydrophobic π-π interactions in the reactive surface of these nanomaterials. In addition, previous studies show that the graphene functionalization-based oxidation processes significantly increase the absorption properties. Because oxidized-surface moieties (epoxy, OH and COOH) present in the oxidized-Gr reactive surface present high-affinity to strongly interact with polycyclic aromatic hydrocarbons (PAHs).[11,12]

In this context, the graphene nanostructures, could provide a promising bioremediation alternative for the treatment of water contaminated by oil and its derivatives in overload conditions.[10-12] It is well-known that the specific properties of graphene nanostructures can provide a high adsorption capacity initially coined with the term "*Trojan-horse effect*".[10-15] Several studies have recognized the *Trojan-horse-like effects* induced by carbon nanomaterials as an important mechanism to reduce lethal concentrations and negative impact of many organic pollutants on the environmental compartment (soil and water).[15] Particularly, graphene nanostructures (pristine-Gr and oxidized-Gr) present a high adsorption ability, which is intentionally employed in several applications involving molecular recognition, nanomedicine, and bioremediation.[14-18]

Theoretical studies have been proposed, in this work, based on environmental modeling and simulations, that can qualitatively reproduce the complex processes that occur in the environmental compartments using mathematical and physical models to describe the dynamic of the systems and to predict their behavior. At present there are no studies in the literature addressing the analysis of protein-ligand and ligand-ligand interactions on detoxifying proteins and multiple-ligand-like (environmental pollutants) with a heterogeneous environment. For this purpose, the present study propose, for the first time, a new computational approach on the outer membrane protein transport (TodX) from the detoxifying microorganism (*Pseudomonas putida*) interacting with oil-derived hydrocarbons (n-butylbenzene, n-octane and methylnaphthalene) and graphene nanostructures (pristine-Gr and oxidized-Gr) to mimicking overload conditions, like oil-spill by using a new multicomponent docking approach with *ab initio* Density Functional Theory (DFT), in order to tackle the theoretical study on bioremediation strategies.[14-19] In this regard, the present study propose new relevant information underlying the mechanisms of

environmental co-exposure, and, at the same time, open new horizons for the nanotechnology applications in the context of environmental modeling and health safety.

Materials and Methods

Performing the TodX actives binding-sites prediction

The potential TodX binding-sites were predicted through DeepSite[20], which identify TodX-cavities as relevant catalytic sites that is likely to bind to a small ligand into the Van der Waals surfaces. To this end, DeepSite considers all the molecular descriptor related to the proteins TodX using machine-learning algorithm based on 3D-deep convolutional neural networks (DCNNs).[20] The DeepSite method is a robust and validated deep learning library with an extensive test set based on > 6500 proteins of the scPDB database which allows an unequivocal identification of the catalytic binding site in any protein. In this regard, the binding pocket predictions, as well as, the TodX mesh volumetric-map obtained from DeepSite was used to establish the cartesian coordinates of the docking box simulation like TodX grid box size, with X = 22 Å, Y = 18 Å, Z = 32Å dimensions and with TodX-box simulation center as X = 29.615 Å, Y = 63.638 Å and Z = 28.934 Å, with option of exhaustiveness of 100 (average precision).[21, 22]

Crystallographic validation-based on Ramachandran plot

To validate the 3D x-ray crystallographic structure of the transport protein *Pseudomonas putida* (TodX) pdb.model the Ramachandran plot as a general case and the corresponding quality assessment was performed.[23] In order to prevent obtaining false positives on flexible-docking complexes. This methodology allows to verify the absence of restricted-flexibility for each residue from the TodX protein based on the identification of allowed and disallowed torsion values of Ψ (*Psi*) versus Φ (*Phi*).

Elastic network approach on TodX binding sites

This computational algorithm evaluates the signal communication efficiency between two or more binding active site of a given protein (TodX) by describing the residues network communication like Hookean potential (or 'springs') based on elastic normal mode (ENM) analysis of the interaction potential (*U*) obtained from the different sites.[24-26] The mathematical framework of this approach will be discussed in details in the next section.

Molecular docking approach with multicomponent binding systems

In order to study the binding-interactions between the ligands (*i.e..,* oil-derived hydrocarbons: n-butylbenzene, n-octane and methylnaphthalene and the graphene nanostructures: pristine-Gr and oxidized-Gr) with the outer membrane toluene transporter (TodX) from *Pseudomonas putida.* The 3D-crytallographic structure file like TodX protein was retrieved from the RCSB Protein Data Bank (PDB) like PDB ID: 3BRZ with resolution of 3.2 Å.[27] Before the docking approach, the TodX-protein was optimized by using the AutoDock Tools 4 software for AutoDock Vina.[27-29]

Next, the TodX-hydrogen atoms were added according to appropriate hybridization geometry by adding the Gasteiger partial atomic charges, protonation states followed by bond orders assignment and rotatable bonds of the TodX protein.pdb file.[27-30]

Afterward, the ligand structures like: methylnaphthalene (PubChem CID: 7002), n-butylbenzene (PubChem CID: 7705), n-octane (PubChem CID: 356), [32] and the graphene nanostructures (pristine-Gr and oxidized-Gr) like the mol2. input files were optimized by using the MOPAC extension for geometry optimization based on the AM1-Hamiltonian method.[31-32] Herein, it is important to clarify that the toluene ligand even though is the most recognized substrate of the toluene transport protein *Pseudomonas putida* (TodX) we did not take it into account for the purposes of this study, focusing our attention in the hydrophobic oil-derived hydrocarbon TodX substrates with greater degree of environmental persistence and bioaccumulation like methylnaphthalene, n-butylbenzene, and n-octane.[32]

According to the main objective of this work to evaluate the interactions mechanism from the formed complexes, the free energy of binding or affinity (FEB, kcal/mol) was obtained considering the following systems: **i**) TodX + n-butylbenzene, ***ii***) TodX + n-octane, ***iii***) TodX + methylnaphthalene, ***iv***) TodX + Gr-pristine and ***v***) TodX + oxidized-Gr. Furthermore, to mimicking the environmental co-exposure with the oil-derived hydrocarbons with two graphene nanostructures the following two heterogeneous-multicomponent docking systems were considered: ***vi***) TodX + (methylnaphthalene/n-butylbenzene/n-octane) + Gr-pristine and ***vii***) TodX + (methylnaphthalene/n-butylbenzene/n-octane) + oxidized-Gr. For this instance, the Autodock Vina scoring function was implemented.[27] Herein, the implemented the Vina scoring function combines the knowledge-based potential and empirical information from experimentally-validated binding affinity measurements with default Amber force-field thermodynamic parameters.[27-29] For this instance, the Vina scoring function considers optimal-linear Gibbs free energy of binding affinity ($\Delta G \approx$ FEB dock). It is important to note that, overall docking force field parameters are based on distance-dependent atom-pair interactions (d_{ij}). The free energy of binding (FEB kcal/mol as output of docking results) was defined by ΔG_{bind} values for all docked poses (TodX-ligands) like a sum of the individual molecular mechanics terms of standard-chemical potentials as: Van der Waals interactions (ΔG_{vdW}), hydrogen bond ($\Delta G_{H\text{-}bond}$), electrostatic interactions ($\Delta G_{electrost}$), and intra-molecular ligands interactions ($\Delta G_{internal}$).[27-29] See the general thermodynamic **equations (1)** and **(2)**.

$$FEB_{dock} \approx \Delta G_{bind} = \Delta G_{vdW} + \Delta G_{H-bond} + \Delta G_{eletrost} + \Delta G_{int} \quad \mathbf{(1)}$$

$$\mathrm{FEB}_{dock} \approx \Delta \mathrm{G}_{bind} = \Delta \mathrm{G}_{VdW} \sum_{lig-\mathrm{TodX}} \left(\frac{A_{ij}}{{d_{ij}}^{12}} - \frac{B_{ij}}{{d_{ij}}^{6}}\right) + \Delta \mathrm{G}_{H-bond} \sum_{lig-\mathrm{TodX}} E(t) \left(\frac{C_{ij}}{{d_{ij}}^{12}} - \frac{D_{ij}}{{d_{ij}}^{10}}\right) + \Delta G_{elec} \sum_{lig-\mathrm{TodX}} 332.0 \frac{q_i q_j}{\epsilon(d_{ij}) d_{ij}} + \Delta G_{int} \left\{\sum_{lig} \frac{A_{ij}}{{d_{ij}}^{12}} - \frac{B_{ij}}{{d_{ij}}^{6}} + \sum_{lig} E(t) \times \left(\frac{C_{ij}}{{d_{ij}}^{12}} - \frac{D_{ij}}{{d_{ij}}^{10}}\right) + \sum_{lig} 332.0 \frac{q_i q_j}{4 d_{ij} d_{ij}} + \sum_{lig} \gamma_k \left(1 + \cos(\omega_k \theta_k - \theta_{0k})\right) \quad \mathbf{(2)}$$

The affinity (ΔG_{bind}) values obtained from the docking complexes were categorized-like energetically-unfavorable when the $\Delta G_{bind} \geq 0$ kcal/mol, indicating an either extremely low or complete absence of affinity of the oil-derived hydrocarbons and/or graphene nanostructure interaction complexes; otherwise are categorized-like medium to high-affinity of binding. Additional details on the thermodynamic force field parameters used in this study can be consulted in Autodock Vina scoring function.[27-39]

By the other hand, the ligand conformations with the lowest Gibbs free energies of binding (*i.e.,* the more negatives FEB values) were retrieved like outputs. The best root-mean-square deviation (*R.M.S.D*) was considered as a criterion of correct docking pose accuracy below 2Å according to the **equation (3)**.

$$RMSD\left(pose_{i-lig}, pose_{j-\mathrm{TodX}}\right) = \sqrt{\frac{\sum n\left(\left(atom_{(i-lig)}\right)-\left(atom_{(j-TodX)}\right)\right)^2}{n}} \qquad \textbf{(3)}$$

Ab initio simulation

The *ab initio* DFT methodology, implemented with the SIESTA code (Spanish Initiative for Electronic Simulations with Thousands of Atoms)[41], was used combined with docking simulation experiments. In this regard, two DFT-simulation groups presenting the most stable binding configuration three DFT-interacting systems each one were considered like: **Group #1**: ***i***) pristine-Gr + n-butylbenzene, ***ii***) pristine-Gr + n-octane, ***iii***) pristine-Gr + methylnaphthalene and the **Group #2**: ***i***) oxidized-Gr + n-butylbenzene, ***ii***) oxidized-Gr + n-octane, ***iii***) oxidized-Gr + methylnaphthalene considering the optimized systems obtained from the most stable final configuration. For this instance, DFT-algorithm performs self-consistent calculations to solve the Kohn-Sham equation and evaluates the resulting properties of the interactions studied.[42] For this instance, double-base function polarized (DZP) was used for the exchange-correlation potential using a Local Density Approximation (LDA) parameterized by Perdew and Zunger[43] with cutting radius of 300 Ry for the mesh (grid) of the real space interaction. The atomic structures were relaxed until the residual forces were less than 0.05 eV / Å for all the atoms of the system. The interactions between the valence electrons and the ionic core was treated within the pseudopotential method as proposed by Troullier and Martins.[44] For each DFT-simulation group (**Group #1 and Group #2**), several DFT-parameters were evaluated namely: the interaction energy of the ligands like (E_b), smallest interatomic distance (d), and the charge transfer (ΔQ). Furthermore, the electronic band structures, as well as, the associated conduction band minimum (CBM) and the valence band maximum (VBM), with respect to the Fermi level were determined in the cases of graphene nanostructures (pristine-Gr and oxidized-Gr). By the other hand, in the case of the oil-derived-hydrocarbons (methylnaphthalene, n-butylbenzene or n-octane) the associated energy difference between the highest occupied molecular orbital and the lowest unoccupied molecular orbital (HOMO-

LUMO gap energy) was obtained. For this instance, the binding energy (E_b) of the cited DFT-interacting systems were calculated according to the following **equation 4**:

$$E_b = -\{E(A+B) - E(A) - E(B)\} \quad (\mathbf{4})$$

Where, the term E(A+B) is the total energy of the interaction between an evaluated hydrocarbon (methylnaphthalene, n-butylbenzene or n-octane) with a graphene nanostructure (pristine-Gr or oxidized-Gr), the term E(A), represents the total energy of an isolated hydrocarbon molecule, and the last E(B) corresponds to the total energy of the isolated graphene nanostructure.

Results and discussion

Bacterial biodegradation of oil-derived hydrocarbons is a novel and important process for environmental remediation, which requires the hydrophobic transport of these compounds across the bacterial cell membrane. In this regard, we report for the first time a computational study toward to improve the current knowledge about environmental detoxification mechanisms using *Pseudomonas putida*.[6-10] Specifically, the modeling of interactions of the outer membrane transport protein TodX, which have been implicated in the passage of hydrophobic molecules and biodegradation of oil-derived hydrocarbons from the extracellular environment towards the periplasm.[6-10] In this regard, we carried out a theoretical modeling by adapting the traditional molecular docking procedures by performing a new heterogeneous multicomponent docking approach in accordance with our objective.[33,34] Then, we assume that the canonical ligand-protein (1:1) proportion (*i.e.,* one hydrocarbons molecule: one protein TodX) fit with under-exposure conditions with easy biodegradation by TodX.[22,28,29]

On the other hand, we considered the modeling based on the heterogeneous mixture of oil-derived hydrocarbons like methylnaphthalene, n-butylbenzene and n-octane in the multicomponent ligand-protein evaluation. Mimicking environmental overload conditions (high hydrocarbon concentrations).[33,34] In this context, we introduce graphene nanostructures to tackle the docking and DFT study to model potential physico-chemical adsorption of the cited oil-derived hydrocarbons concomitantly interacting with the transport protein TodX in equilibrium conditions.[33,34]

To start the study, one of the most important steps to ensure quality of modeling data consists in the prediction/identification of the suitable TodX binding-sites along with an appropriate crystallographic-structural validation and flexibility properties of this protein. In this concern, in the present work the TodX binding-sites predictions were carried out by applying *ezPocket* package which use Voronoi tessellation method to detect tiny cavities and collecting information-based crystallographic descriptors about the pocket topology with high probability to bind small ligands.[20,21] The binding cavity detection method (*fpocket*) generates cartesian coordinates-like volumetric maps that allows setting the docking box-simulation on the TodX binding site. For this instances to binding sites were identified like: TodX_Site 1 grid box-size with dimensions of X= 54 Å, Y= 54 Å, Z= 54 Å

and TodX grid box-center X= 31.08 Å, Y= 23.18 Å, Z = 51.41 Å with volume of 769.92 Å^3 and the TodX_Site 2 grid box-size with dimensions of X= 64 Å, Y= 64 Å, Z= 64 Å and TodX grid box-center X= 26.43 Å, Y= 47.63 Å, Z = 27.09 Å with volume of 3846.61 Å^3. [20,21] Furthermore, the flexibility properties and collective motions-like anisotropic fluctuations were evaluated from the whole TodX structure.[24-26] See **Figure 1**.

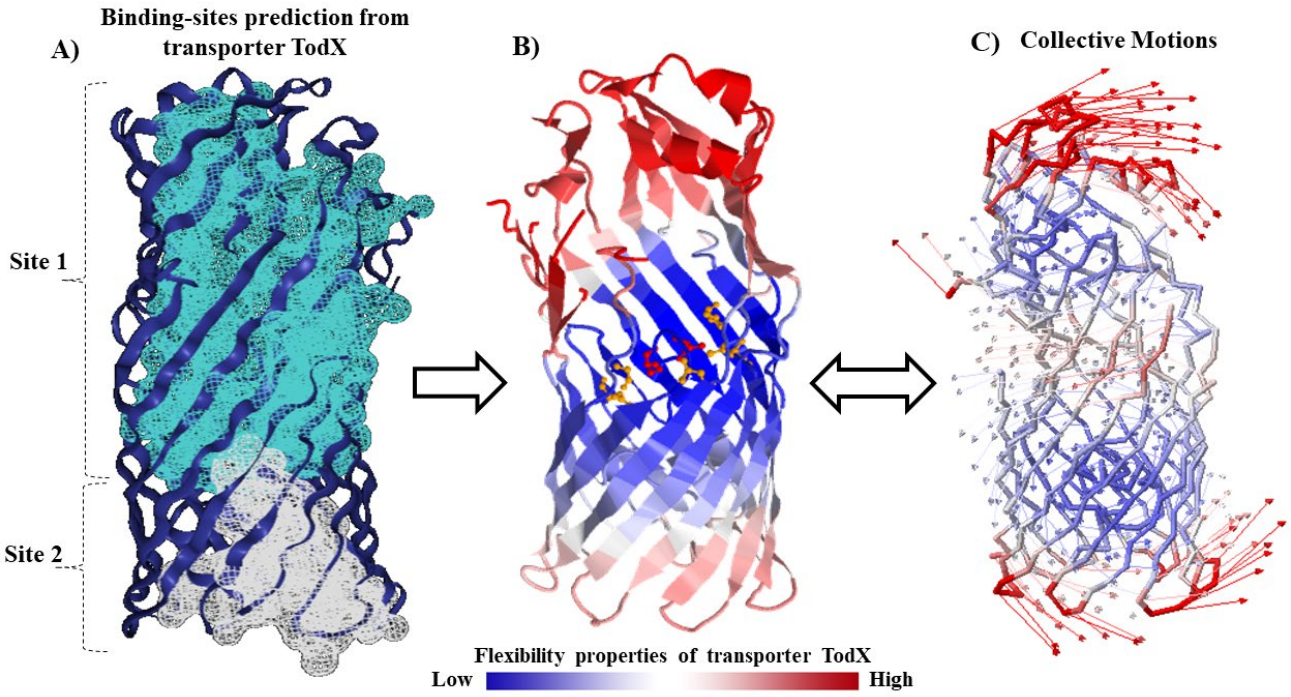

Figure 1. ***A)*** *Representation of ezPocket calculation/prediction of topological-cavities like embedded-membrane binding site 1 (light blue) and extracellular domain also named hatch domain or site 2 (white) from the outer membrane transport protein (TodX) family from Pseudomonas putida represented as volumetric Van der Waals surface/mesh representation.* ***B)*** *Representation of TodX flexibility properties like 3D-colored structure based on the size of fluctuations-driven according to the slowest vibration-modes from TodX-residues from low-flexibility (blue) to high-flexibility (red). Herein, the catalytic binding residues are in the region of the site 1 in the middle of the channel labeled-yellow and red.* ***C)*** *On the far right, atomic positional fluctuations illustrating the correlated motions between the two previously identified binding sites like site 1 and site 2.*

Afterward, to validate the 3D-X-ray crystallographic structure of the TodX-structure the Ramachandran plot diagram coupled to quality assessment was performed to avoid false positives in the flexible docking results.[23] See **Figure 2**.

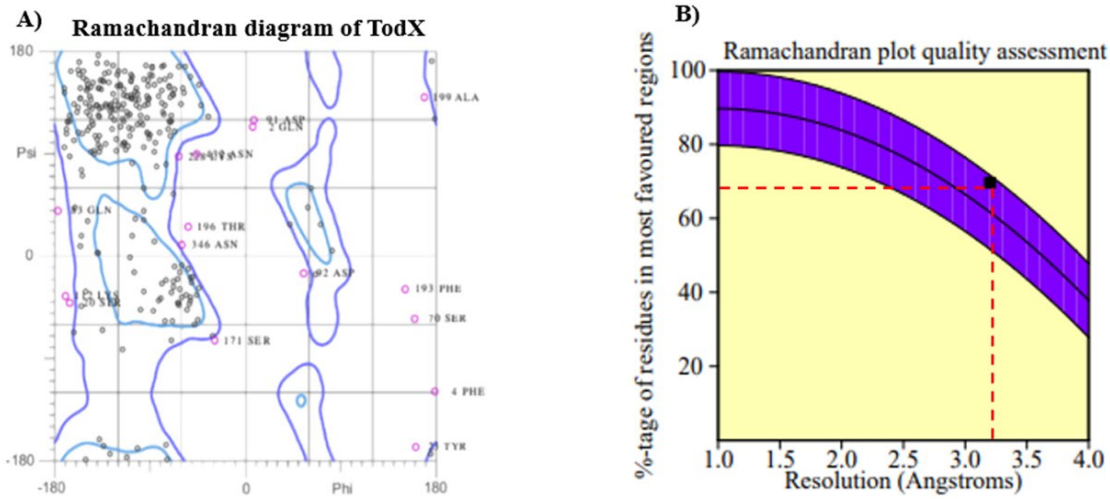

Figure 2. ***A)*** *Representation of Ramachandran analysis with the spatial distribution of Ramachandran outliers (pink balls) in the modeled pdb x-ray structure of TodX protein. All the possible combinations of dihedral angles of torsion like Psi vs. Phi of each amino acid residue of TodX are showed.* ***B)*** *Results of Ramachandran quality assessment (3brz.pdb model quality) measured by the percentage of the TodX-residues which are in the most favored, or core, regions of the Ramachandran plot vs. resolution (Å). For this instance, the TodX crystallographic structure exhibits an acceptable crystallographic quality with more than 70% of the residues placed in the favored region including the site 1 and site 2 (red-dotted line).*

Ramachandran evaluation is a 2D-projection on the plane from the 3D-crystallographic TodX model.pdb where all the possible TodX binding sites conformations of each residue are defined into the plot according to the torsion dihedral angles Psi *vs.* Phi around the TodX peptide-bond residues.[23] In this context, allowed torsion values of the cited dihedral angles are placed within the Ramachandran colored purple contour (as conformational-favored TodX-residues).[23] Otherwise, are considered as TodX-sterically-disallowed residue associated with torsion values of dihedral angles Psi *vs.* Phi which appear outside of the Ramachandran colored purple contour (like conformational non-favored amino acid residues). Following the sequence of modeling interactions, we performed the *in silico* experiment in order to get the free energy of binding (FEB, kcal/mol) for the complexes formed between the TodX protein and the oil-derived hydrocarbons, mimicking low or high-concentration in the absence or presence of graphene nanostructure (pristine-Gr and oxidized-Gr).

Herein, it is important to refer some environmental issues that surrounding environmental processes before moving directly to models these complex interactions. In this sense, for the best of our knowledge, there is no evidences considering the environmental modeling using graphene nanostructure with detoxifying microorganisms. Although there are very interesting works based on experimental nanoecotoxicological evaluations, which have been able to reproduce with a certain level of precision the *Trojan-horse phenomenon* induced by carbon nanomaterials in co-exposure conditions.[15]

Firstly, was performed the flexible docking interaction mimicking low hydrocarbons concentrations.[29-34] Hydrocarbons that derived from petroleum such as oil, gasoline, and diesel-fuel are among the most commonly occurring and widely-used contaminants in the environment.[45] Crude oil occurs inside the earth and is composed by a complex mixture of natural compounds composed mostly of hydrocarbons containing only H-atom and C-atoms. The remaining elements of sulfur, nitrogen, and oxygen are less than 3% of the petroleum.[45,46] Petroleum oil-derived products are released within the environment accidentally and intentionally at all steps of its use like exploration, production, transportation, storage, use and disposal. The most volatile subcomponents of petroleum are biodistributed preferentially into the atmosphere and hydrosphere inducing the well-known bioaccumulation and bioconcentration processes which exceed the biotransformation capacity of the of the environmental compartments mainly water or can impact the trophic chains (including the Homo sapiens trophic chain) by inducing the biomagnification process in the most of cases.[47-49] This event can be defined like the increase of the concentration of pollutant (oil-derived hydrocarbons) through the different levels of the trophic chain. [47-49] Then, after defining this ecotoxicological concepts we can pass to explain our computational approaches.

It is important to note that the low-concentration condition was modeled according to the theoretical protein : ligand proportion (1:1) (*ie.,* one hydrocarbons molecule: one protein TodX) mimicking an easy biodegradation by TodX (*ie.,* docking interaction with the previously predicted catalytic binding residues in the TodX site 1) not involving potential hydrocarbon-hydrocarbon interactions as usually happens in mixtures released into the environment in high-concentration. The results of the flexible docking procedures applied are depicted in the **Figure 3**

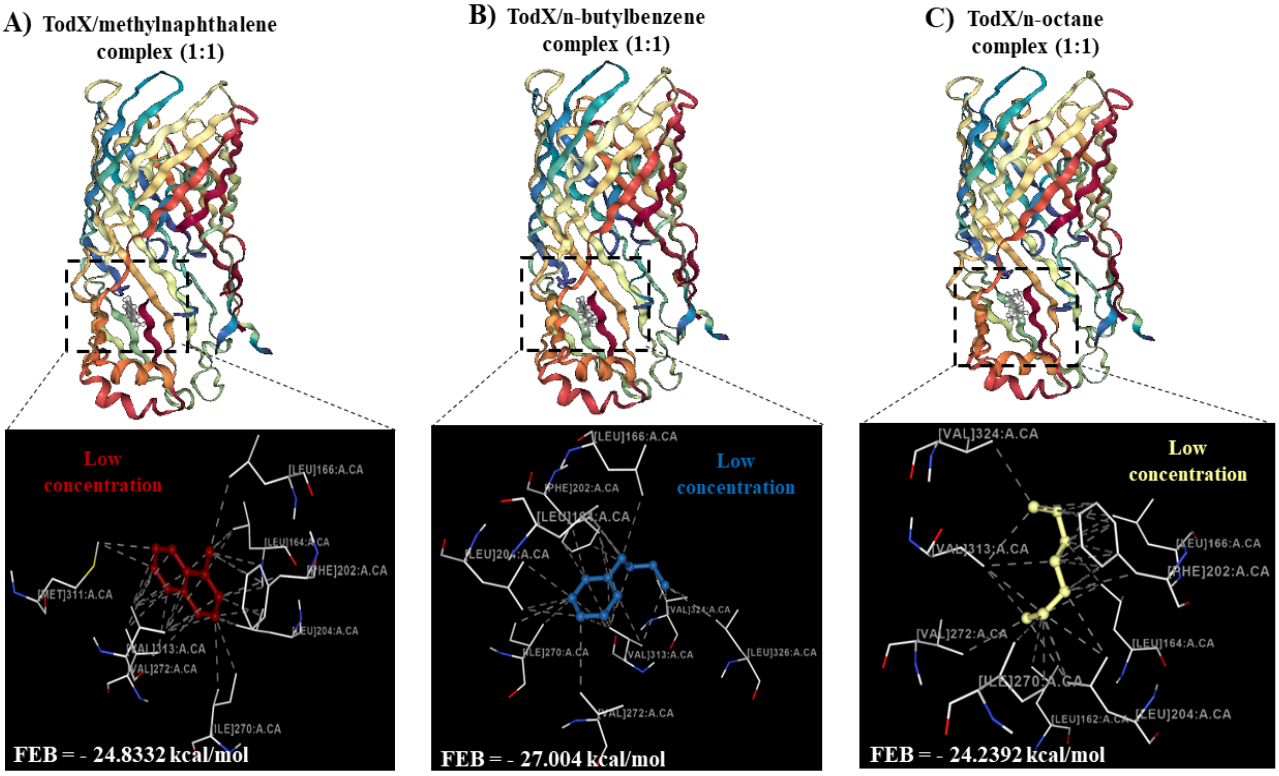

Figure 3. *On the top, representation for each hydrocarbon/TodX docking complexes obtained for the best crystallographic-docking pose (RMSD < 2Å) using flexible molecular docking mimicking low hydrocarbon concentration (i.e., ligand-protein 1:1 proportion) in the TodX catalytic binding site 1.* ***A)*** *FEB (TodX/methylnaphtalene complex) = - 24.8332 kcal/mol with RMSD = 0.731Å,* ***B)*** *FEB (TodX/n-butylbenzene complex) = -27.004 kcal/mol with RMSD = 0.46Å,* ***C)*** *FEB (TodX/n-octane complex) = -24.2392 kcal/mol with RMSD = 0.72Å. On the bottom, representation of the corresponding 3D-lig-plot diagrams of interactions from the docking complex showing multiple hydrophobic interactions (gray dotted lines). For this instance, a color-label is assigned for each hydrocarbon like methylnaphthalene (red), n-butylbenzene (blue) and n-octane (yellow).*

Following this idea, we carried out the same docking simulation experiments using the two graphene nanostructures like pristine-Gr and oxidized-Gr in order to theoretically verify the interaction behavior of these systems mimicking low-concentrations.[29-34] See **Figure 4**.

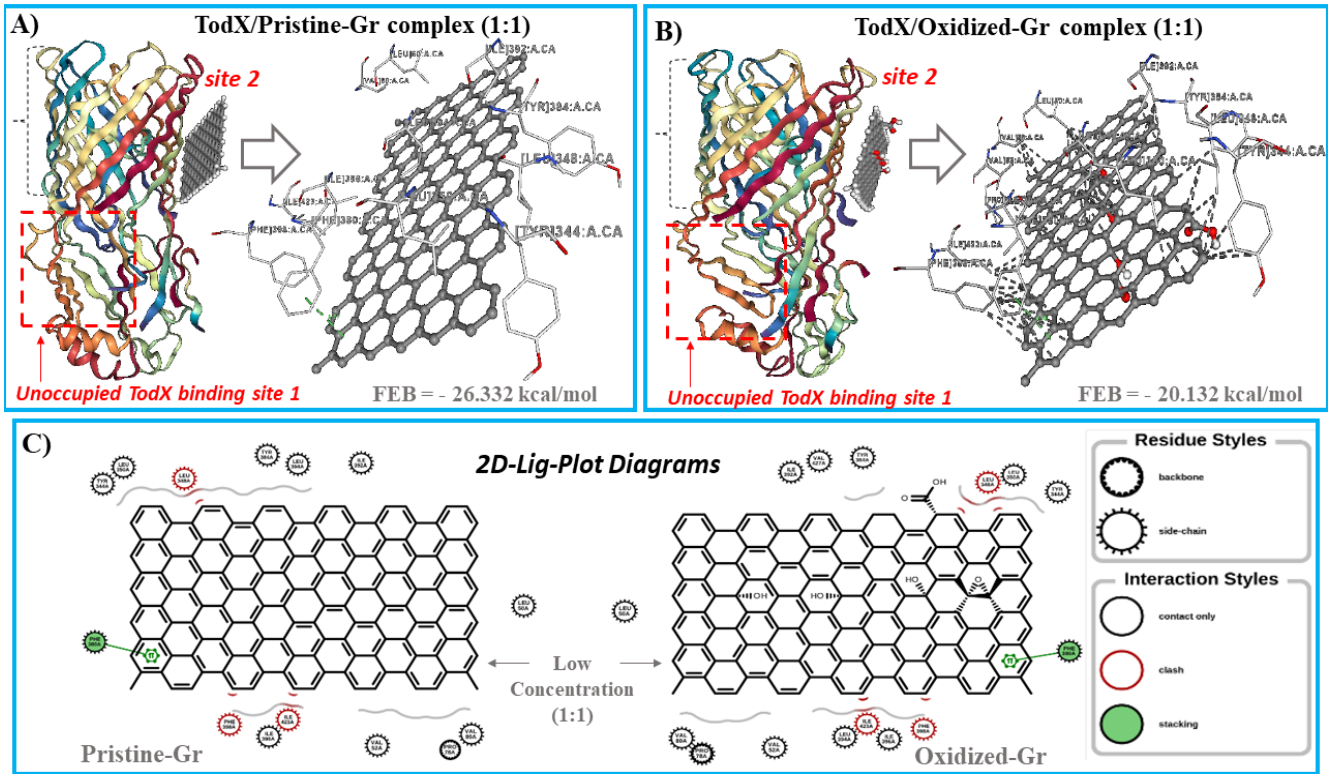

Figure 4. *On the top, representation for each graphene nanostructure/TodX docking complexes obtained for the best crystallographic-docking pose (RMSD < 2Å) applying flexible molecular docking modeling the behavior of low graphene nanostructure concentrations (i.e., ligand-protein 1:1 proportion) in the TodX binding site 2, Please, note that the catalytic site 1 remains unoccupied for both carbon nanomaterials.* ***A)*** *FEB (TodX/pristine-Gr complex) = - 26.332 kcal/mol with RMSD = 1.431Å,* ***B)*** *FEB (TodX/oxidized-Gr complex) = -20.132 kcal/mol with RMSD = 1.406Å, in both panels are depicted on the right side, the corresponding 3D-lig-plot diagrams of the aforementioned docking complex showing multiple non-covalent hydrophobic interactions (gray dotted lines) highlighting the surrounding TodX-target amino acid residues from the site 2. On the bottom,* ***C)*** *Additional*

representation like 2D-lig-plot diagrams of interactions obtained from the cited docking complexes for pristine-Gr (left-side) and oxidized-Gr (right-site). Note the presence of multiple non-covalent hydrophobic interactions based on hydrophobic (N···C···C)-backbone together with side-chain contacts, a unique π–π stacking interaction with Phe 398-TodX (green) and several steric clashes (red).

According to these results, we suggest that the interactions of graphene nanostructure in low-concentrations occour in a different biophysical environment, involving lateral non-covalent hydrophobic contacts which, mainly affect the target residues from the extracellular domain binding site 2 according to (N···C···C)-backbone and side chains (A) interactions.[47-49] Then, considering that the biophysical environment of the interaction for the oil-derived hydrocarbons is placed in the TodX site 1 faraway of the TodX site 2, we strongly suggest that the biodegradation ability of the TodX protein could be partially affected under co-exposure with pristine-Gr and oxidized-Gr in low-concentration.

In this context, to evaluate the communication efficiency between the TodX binding site 1 and site 2 we carried out the ENM approach considering the collective motions in the TodX residue network (refer **Figure 1C**). The ENM analysis, allows the representation of the communication strength that each TodX residue has over every neighbor's residue (*i.e.,* residues from site 1 ↔ residues from site 2) based on the linear response theory.[24-26] For this instance, the collective fluctuation of the anisotropic network is defined by the $3N \times 3N$ Hessian matrix (H) following **equation 5**:

$$C_{i,j} = \begin{bmatrix} C_{1,1} & C_{1,2} & \cdots\cdots\cdots & C_{1,N} \\ C_{2,1} & C_{2,2} & \cdots\cdots\cdots & C_{2,N} \\ . & . & \cdots\cdots\cdots & . \\ C_{N,1} & C_{N,2} & \cdots\cdots\cdots & C_{N,N} \end{bmatrix} \textbf{(5)}$$

Where elements ($1 \leq i, j \leq N$) are the second derivatives of the ENM network potential (U) from **equation 6**:

$$C_{i,j} = \begin{bmatrix} \partial^2 U/\partial X_i \partial X_j & \partial^2 U/\partial X_i \partial Y_j & \partial^2 U/\partial X_i \partial Z_j \\ \partial^2 U/\partial Y_i X_j & \partial^2 U/\partial Y_i \partial Y_j & \partial^2 U/\partial Y_i \partial Z_j \\ \partial^2 U/\partial Z_i X_j & \partial^2 U/\partial Z_i \partial Y_j & \partial^2 U/\partial Z_i \partial Z_j \end{bmatrix} \textbf{(6)}$$

Herein, we use the biophysical parameter Markov commute-time [C (i, j) ↔ C (j, i)][24-26] to represent the ability of a given structurally communicated TodX binding residues (i, j) to receive and send signals in both directions ($j \rightarrow i$ and $i \rightarrow j$) from the site 1 to site 2 and vice versa. See **Figure 5**.

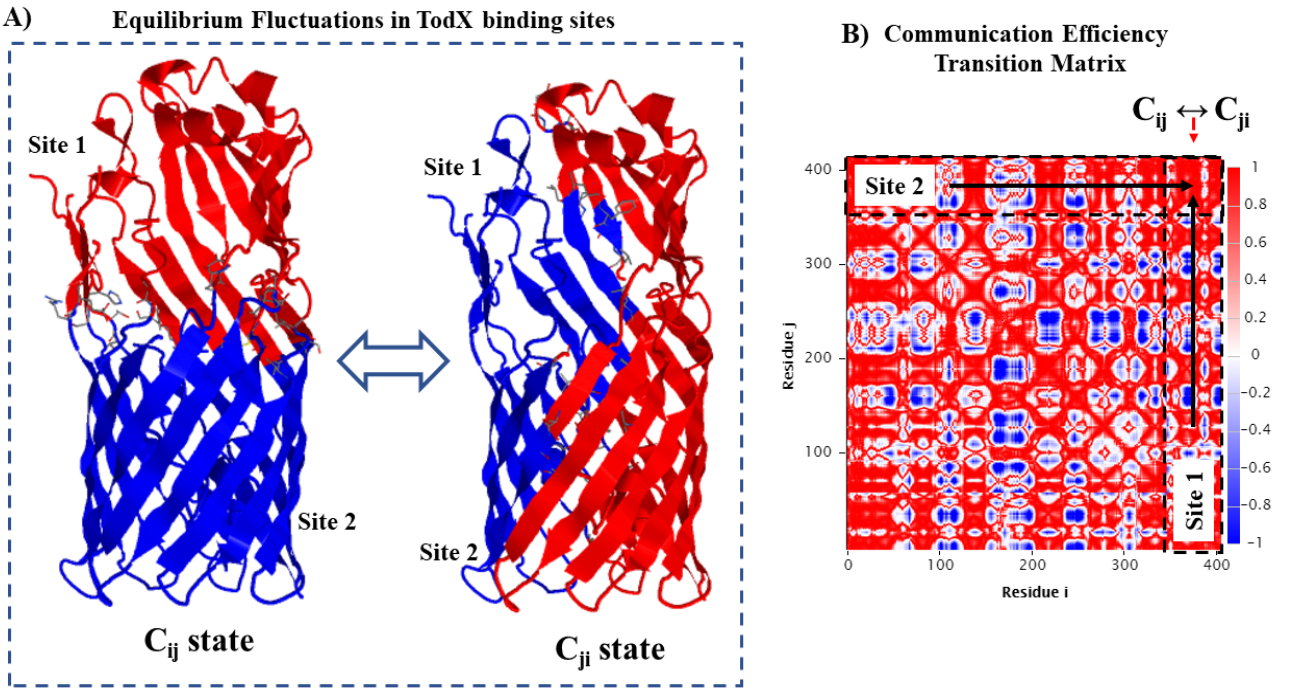

Figure 5. *On the left,* ***A)*** *the 3D-cartoon representation of the inter-communication of TodX binding sites (site 1 and site 2) according to the different coupling states ([C (i, j) ↔ C (j, i)]) based on ENM approach.* ***B)*** *On the right, the corresponding two-dimensional communication efficiency transition matrix network-based on Markov commute time (C (i, j)), clustering receiving and communicating residues from the site 1 and site 2 of the TodX protein are represented by black-dotted rectangles. The color bar on the right side of the map indicates the pairs of TodX residues (i, j) that present fully correlated motions or strong correlations (0.2 ≤ (C_{ij}↔C_{ji}) ≤ 1) with labeled-color red indicating the same direction for the i and j residues-fluctuation, while the fluctuations based on anti-correlated motions of (i, j)-residue (i.e.: C_{ij}↔C_{ji} ≤ 0) are colored in blue (opposite-direction for the fluctuation-motions of residues i and j) and the moderately correlated and uncorrelated (C_{ij}↔C_{ji} ≈ 0) regions are labeled by light red and blue color, respectively.*

The map of signal communication efficiency of TodX binding sites provides relevant information regarding the effective communication distances-based on the Markov commute time parameter (C (*i, j*)) for intra-segment C*α*-C*α* atomic distance fluctuations, which can be categorized like: *i)* fluctuations-based distances involving short segments (# TodX residues: 10–22), *ii)* fluctuations-based distance from medium segments (# TodX residues: 23–26) and *iii)* fluctuations-based distance from long segments (TodX residues: 27–50).[50] Then, considering the results of the ENM approach we observe the presence of TodX-residues fluctuations involving coupled motion from medium to long distances based on the C_{ij}↔C_{ji} parameter.[24-26] This approach suggests that both graphene nanostructures pristine-Gr that interacts with target residues (Phe398, Ile423, Ile396, Phe380, Val80, Leu50, Leu394, Leu350, Tyr384, Leu348, Tyr344) and the oxidized-Gr that interacts with target residues (Phe398, Ile423, Phe380, Ile396, Pro78, Val52, Val80, Leu50, Leu394, Ile392, Leu350, Tyr384, Leu348, Tyr344) in the extra-cellular site

2 (Refer to **Figure 1**). These fluctuations can induce potential perturbations in the biophysical environment of the site 1, where the main TodX catalytic residues are placed, and consequently could affect the biodegradation of the oil-derived hydrocarbon (n-butylbenzene, n-octane and methylnaphthalene) despite under low-concentration (1:1 protein-ligand proportion).[24-26]

The use of computational tools has been recommended and recognized by major regulatory agencies including the Organization for Economic Cooperation and Development (OECD, 2009)[51-54] and the International Organization for Standardization (ISO/TC 229, 2011)[51-54] based on the importance of developing alternative methods in nano-ecotoxicology.[51-54] The present docking approach try to offers a conceptual vision on the co-exposure phenomena, which are largely ignored from the theoretical point of view in nanoecotoxicological evaluations. The most studies address these environmental problems are carried out by performing predictive NanoQSAR models (Nano-Quantitative-Structure-Activity-Relationships).[55] While mechanistic studies-based on multiple ligand-protein interactions explaining thermodynamic aspects of the carbon nanomaterial (in high-concentrations) remain unexplored until the present.

Following this idea, we carried out the simulation experiments considering simultaneous docking interactions, in order to theoretically model co-exposure conditions in high concentrations of the oil-derived hydrocarbons forming mixtures in the absence and the presence of detoxifying TodX protein and both graphene nanostructure (pristine-Gr and oxidized-Gr). Herein, the theoretical ecotoxicological response will depend on the ligand concentration (*i.e.,* ligand proportion stablished) and on the affinity-based energy difference for the ligands bound and/or unbound with the TodX protein. Following this idea, first, we will focus on the bound state in the presence of TodX protein and the graphene nanostructures mimicking co-exposure with oil-derived hydrocarbon in overload conditions.[33,34] As mentioned above the TodX protein allows the lateral diffusion of hydrophobic substrates through the previously identified site 1 under normal conditions.[9] In this regard, the crystal structure of TodX protein from *Pseudomonas putida* shows that the opening in the wall of the beta-barrel is conserved composed by a long hydrophobic tunnel, which mediate the substrate passage from the extracellular environment, through a polar lipopolysaccharide layer and, through of the lateral opening in the barrel wall (embedded-membrane site 1), inside the lipid bilayer allowing the hydrophobic substrate diffusion into the periplasm.[9,10] However, under high oil-derived hydrocarbon concentrations and/or co-exposure conditions of interactions the biotransformation capacity is severely compromised, due to the saturation processes in the main catalytic residues composing the site 1, increasing the likelihood of inducing the loss of detoxifying ability linked to TodX channel nanotoxicity, the intensity of the response will depend on the hydrocarbon concentration and on the energy difference for a given hydrocarbon to be bound (*b*) or unbound (*unb*) with the TodX-protein.[27,33,34] Herein, considering the complexity of the problem of high hydrocarbon concentrations interacting with the TodX, and regarding that the total affinity (ΔG_{bind}) of the oil-derived hydrocarbons by TodX (catalytic site 1) can be modulated in the presence of carbon nanomaterials like graphene nanostructures, we carried out a molecular docking approach-based on

Boltzmann multiplicity states.[27,33,34] For this instance, we can define the hydrocarbon overload interacting with TodX protein like a Boltzmann problem involving TodX channel nanotoxicity (*i.e.,* TodX site 1 saturation-induced by oil-derived hydrocarbons: methylnaphthalene, n-butylbenzene, n-octane and the graphene nanostructures: pristine-Gr and oxidized-Gr). Where the unbound state of oil-derived hydrocarbons and the graphene nanostructures in solution has a total unbound energy like $\varepsilon_{unb\_total} = \sum(\sum\varepsilon_{unb\ hydrocarbons} + \sum\varepsilon_{unb\ graphenes})$ and its corresponding energy $\varepsilon_{b\_total} = \sum(\sum\varepsilon_{b\_hydrocarbons} + \sum\varepsilon_{b\_graphenes})$, when forming the docking complexes with the *TodX*-receptor. Then, we can represent the Boltzmann problem-based distribution like an enumeration of multiple substrates (ligands) of docking interactions. See **Figure 6**.

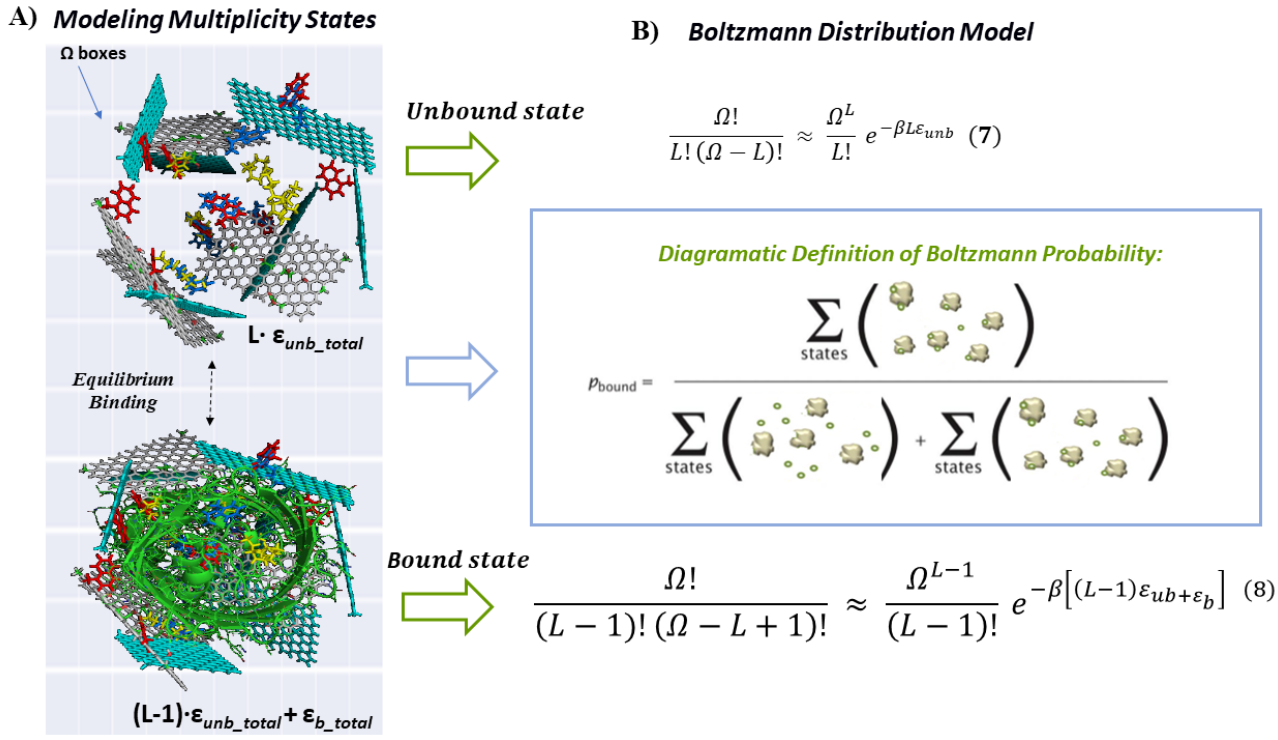

$$\frac{\Omega!}{L!\,(\Omega - L)!} \approx \frac{\Omega^{L}}{L!}\, e^{-\beta L \varepsilon_{unb}} \quad (7)$$

$$p_{bound} = \frac{\sum_{states}(\quad)}{\sum_{states}(\quad) + \sum_{states}(\quad)}$$

$$\frac{\Omega!}{(L-1)!\,(\Omega - L + 1)!} \approx \frac{\Omega^{L-1}}{(L-1)!}\, e^{-\beta\left[(L-1)\varepsilon_{ub} + \varepsilon_{b}\right]} \quad (8)$$

Figure 6. *On the left,* ***A)*** *Representation of molecular docking approach based- Gibbs distribution under co-exposure equilibrium binding in multiplicity states,[33,34] showing the heterogeneous multicomponent docking complex formed by the oil-derived hydrocarbons like methylnaphthalene (red), n-butylbenzene (dark blue), n-octane (yellow), TodX protein (green), and the graphene nanostructures pristine-Gr (light blue) and oxidized-Gr (gray) in the unbound and bound state. On the right,* ***B)*** *Diagrammatic definition of the Gibbs distribution or Boltzmann probability (ρ_{bound}) of the system through several possible states.*

Then, we can write the Boltzmann probability-based multiplicity states to represent ligand overload conditions like oil-derived hydrocarbons interacting with TodX and graphene nanostructures following the **equation 9**:

$$\rho_{bound} = \frac{e^{-\frac{\varepsilon_b}{k_B T}} \frac{\Omega^{L-1}}{(L-1)!} e^{-(L-1)\frac{\varepsilon_{unb}}{k_B T}}}{\frac{\Omega^L}{L!} e^{\frac{-L\cdot\varepsilon_{unb}}{k_B T}} + e^{\frac{\varepsilon_{unb}}{k_B T}} \frac{\Omega^{L-1}}{(L-1)!} e^{-(L-1)\frac{\varepsilon_{unb}}{k_B T}}} = \frac{\left(\frac{L}{\Omega}\right) e^{-\Delta\varepsilon/k_B T}}{1 + \left(\left(\frac{L}{\Omega}\right) e^{-\Delta\varepsilon/k_B T}\right)} \quad (\mathbf{9})$$

Herein, L is a function of the ligand concentration (c) under co-exposure conditions with fixed volume (V = 1 nm^3) in the boxes (Ω). In the present study the obtained multicomponent docking complex exhibits macrocanonical collectivity ensemble due to in the modeling systems the chemical potentials, volume (V) and temperature (T) were fixed. Besides, under thermodynamic equilibrium binding we can model these systems in terms of concentration like $c = \frac{L}{V}$ in co-exposure condition with high ligand concentrations. To this end, we can write the ρ_{bound} in term of ligand concentration (c) and equilibrium constant (K_{eq}) following the **equation 10** and **11**:

$$\rho_{bound} = \frac{\left(\frac{c}{c_0}\right) e^{-\frac{\Delta\varepsilon}{k_B T}}}{1 + \left(\frac{c}{c_0}\right)} \quad (\mathbf{10})$$

$$\rho_{bound} = \frac{\left(\frac{c}{K_{eq}}\right)}{1 + \left(\frac{c}{K_{eq}}\right)} \quad (\mathbf{11})$$

Where the $c_0 = \frac{\Omega}{V}$, the $\Delta\varepsilon = \varepsilon_b - \varepsilon_{unb} < 0$; the Boltzmann constant is represented by k_B, the K_{eq} has concentration units and can be expressed as $K_{eq} = c_0 \cdot e^{\frac{\Delta\varepsilon}{kT}}$, where if the $\Omega = 1\ cm^3$ and c_0 = 0.6 M. The Boltzmann probability distribution (ρ_{bound}) shows that states with lower energy will always be more likely to be occupied than states with higher energy. In addition, the ρ_{bound} provides relevant information about the quantitative relationship between the probabilities of the two bounded states (*i.e.,* concomitant interactions of the cited ligands at the same biophysical environment in TodX protein).[33,34] Despite these cases (two bounded-states) have similarities, it is important to distinguish them, since they generalize differently when crucial assumptions are changed. For this instance, under thermodynamic equilibrium binding regarding both energy exchange and ligand exchange, the thermodynamic requirement, fit with a relaxed fixed-composition obtaining a grand-canonical ensemble.[33,34]

According to our results we show that the co-exposure of oil-derived hydrocarbon in overload condition with *Pseudomonas putida* protein (*TodX*) and graphene nanostructures follows a complex multisite binding case. The aforementioned model of multicomponent binding equilibria has been prviously studied, by several authors.[33,34] These theoretical results are included in a theory of Heterogeneous Monod-Wyman-Changeux (HMWC) multicomponent binding systems.[54,56-58] In this context, we can study the heterogeneous multicomponent binding equilibrium constant by modeling the fractional

occupancy or TodX-saturation parameter (δ) as a measure of the affinity constant (*Ki*) to represent the binding of different ligands (oil-derived hydrocarbon and graphene nanostructures) interacting with multiple TodX binding sites (site 1, site 2,..., site$_{(n)}$), also considering non-predicted binding sites. In this regard, the co-exposure scenario and high concentration conditions for multiple ligands (m) (*i.e.,* all the oil-derived hydrocarbon and graphene nanostructures),[54-58] simultaneously interacting with non-identical TodX binding sites (n_k) can be represented according to the **equation 12**:

$$\delta_{TodX\_site} = \frac{1}{n}\frac{\Pi_{k=1}^{m}\left(\sum_{i=1}^{n_k}\left(|X_k|K_i^R\Pi_{j\neq i}\left(1+c_j|X_k|K_j^R\right)\right)\right)+L\Pi_{k=1}^{m}\left(c_i|X_k|K_i^R\Pi_{j\neq i}\left(1+c_j|X_k|K_j^R\right)\right)}{\Pi_{k=1}^{m}\Pi_{i=1}^{n_k}\left(1+|X_k|K_i^R\right)+L\Pi_{k=1}^{m}\Pi_{i=1}^{n_k}\left(1+c_i|X_k|K_i^R\right)} \quad (\mathbf{12})$$

Where the different ligand-affinities are represented by the equilibrium constants (K_i, K_j). The parameter L represent an isomerization constant of the TodX protein take on pseudo-allosteric behavior from $L = \frac{|T_0|}{|R_0|}$, which describe the equilibrium between the high-affinity relaxed state (R_0) and the low-affinity tensor state (T_0) from TodX-binding sites. In this context, the different affinity is represented in the high-affinity R-state (K_i^R) for all the evaluated ligands and the c parameter is associated to how much the equilibrium between T and R states changes under co-exposure conditions.[54,56-59]

Next, we evaluate the energetic contributions for the total affinity (ΔG_{bind}) considering that the ligands binding interactions occur in the high-affinity relaxed conformation state (R_0) of TodX. For this instance, the cases in the absence of the TodX protein will be separately discussed by DFT-simulation. Then, the theoretical results on the formed heterogeneous multicomponent docking complexes are presented below following the order: ***system I***: methylnaphthalene + pristine-Gr + oxidized-Gr, ***system II****:* n-butylbenzene + pristine-Gr + oxidized-Gr, ***system III***: n-octane + pristine-Gr + oxidized-Gr. See the first system in **Figure 7.**

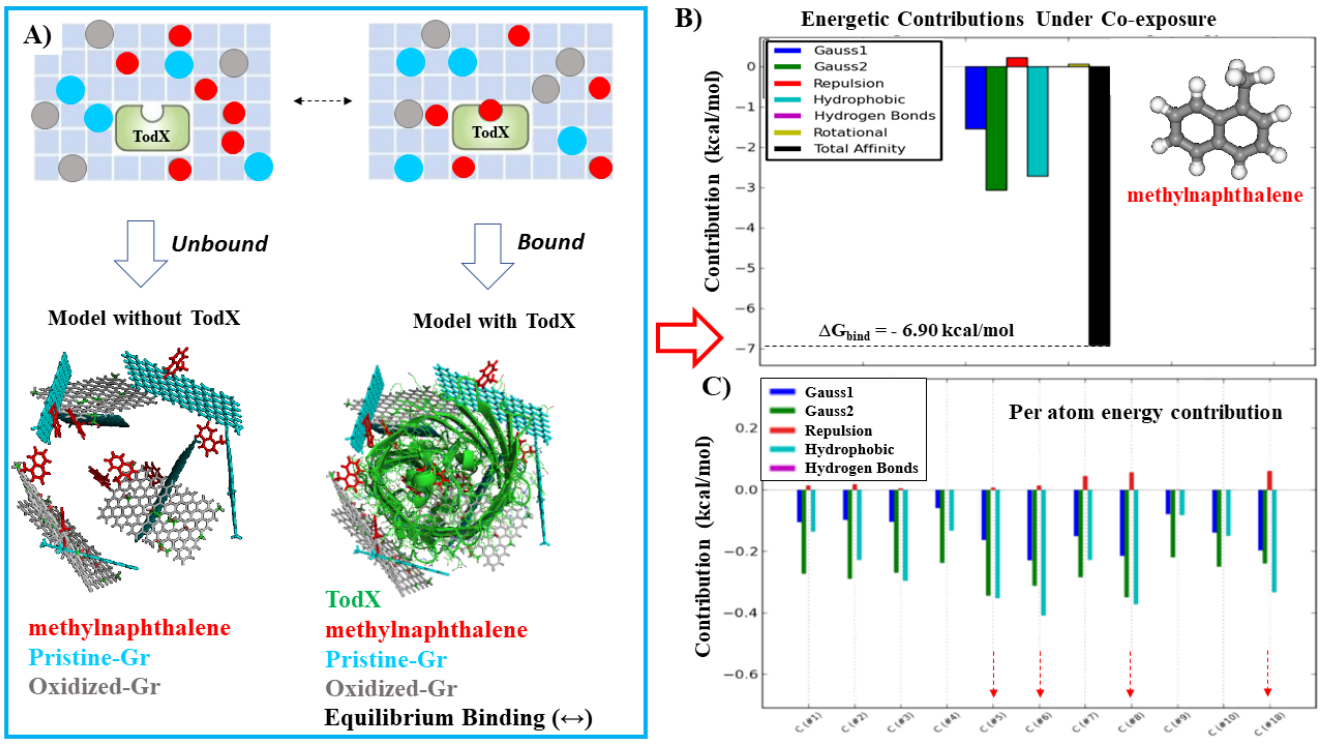

Figure 7. *On the left side,* ***A)*** *Representation of the equilibrium binding-based on the heterogeneous multicomponent docking complex for the* ***system I****: methylnaphthalene (red) + pristine-Gr (light blue) + oxidized-Gr (gray) in high concentration of these ligands. Two co-exposure conditions are represented-like: i) without detoxifying TodX protein and ii) with detoxifying TodX protein. On the upper right side,* ***B)*** *Graphical breakdown of the methylnaphthalene binding energy contributions to the total affinity (ΔG$_{bind}$) with the corresponding values (kcal/mol) under co-exposure conditions with graphene nanostructures pristine-Gr and oxidized-Gr. On the lower right side,* ***C)*** *Graphical representation based on per atom-energy contribution for each methylnaphthalene-atom under co-exposure conditions with graphene nanostructures. For this instance, the methylnaphthalene-atoms with the best contribution to the total affinity (ΔG$_{bind}$) are highlighted (dotted-arrows labeled red) that fit with the light-blue bar for hydrophobic C-atom (C#5, C#6, C#8, and C#18). Herein, the symbol (#) x-axis it was used just for atom-labeling position purposes in the methylnaphthalene structure.*

In the case of the methylnaphthalene, the results show that the most relevant energetic contributions to the total affinity (ΔG$_{bind}$) are provided by a strongest Gaussian molecular mechanism distance-dependent forces (Gauss2) which represent London non-electrostatic attractive energy contributions, followed by the contribution of non-covalent hydrophobic interactions ΔG_{VdW}.[28,37,59] In this regard, the analysis of the maximum atom-energy contribution for the methylnaphthalene shows that the most relevant interacting atoms were the C-atom-labeling positions (C#5, C#6, C#8, and C#18) which provided the strongest hydrophobic interactions. Furthermore, we theoretically suggest that in co-exposure conditions, the presence of graphene nanostructures (pristine-Gr and oxidized-Gr) significantly affected the methylnaphthalene affinity by the detoxifying TodX-protein, according to the results obtained from

the ***system I*** (methylnaphthalene + pristine-Gr + oxidized-Gr + TodX), where the total affinity ΔG_{bind} (methylnaphthalene) = - 6.90 kcal/mol compared with the high-affinity value obtained in low-concentration like 1:1 protein-ligand proportion with ΔG_{bind} (methylnaphthalene/Todx) = -24.8332 kcal/mol (please, refer to **Figure 3A**).

Afterward, we present the ***system II***: n-butylbenzene + pristine-Gr + oxidized-Gr in the **Figure 8.**

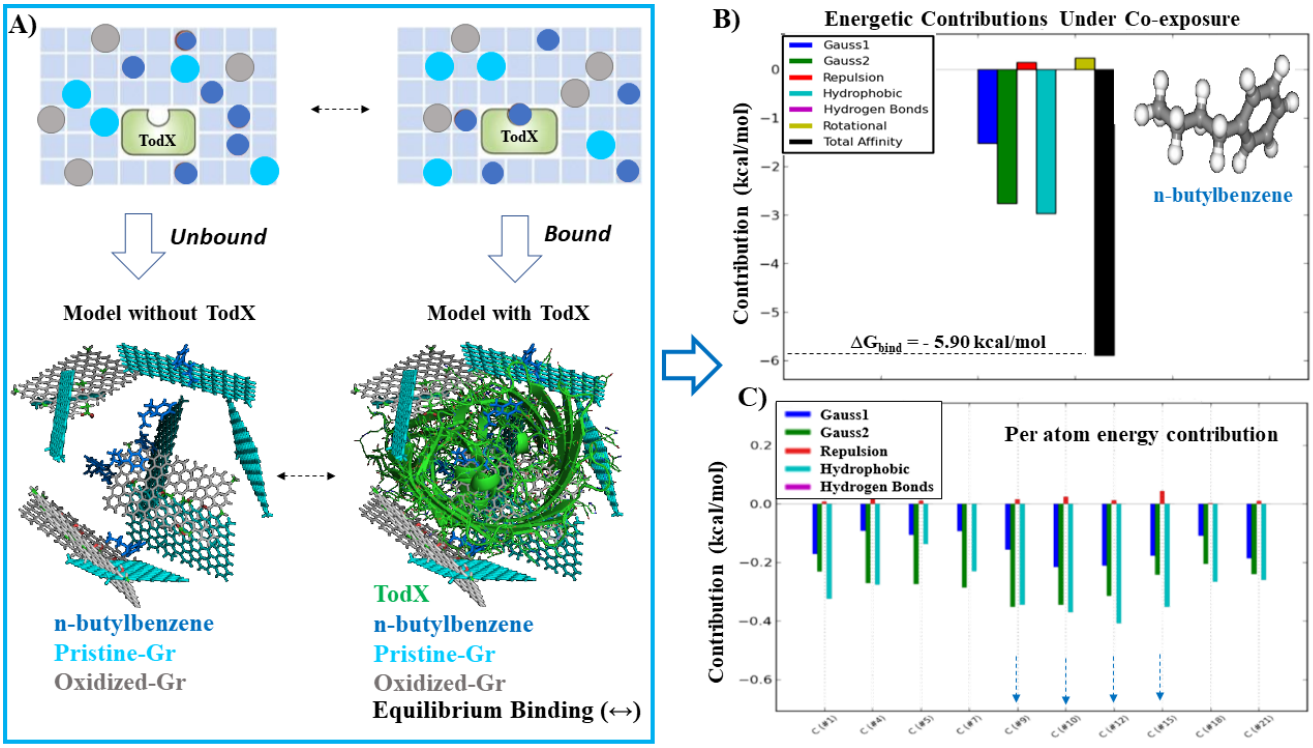

Figure 8. *On the left side,* ***A)*** *Representation of the equilibrium binding-based on the heterogeneous multicomponent docking complex for the* ***system II****: n-butylbenzene (dark blue) + pristine-Gr (light blue) + oxidized-Gr (gray) in a high concentration of these ligands. Two co-exposure conditions are represented-like: i) without detoxifying TodX protein and ii) with detoxifying TodX protein. On the upper right side,* ***B)*** *Graphical breakdown of the n-butylbenzene binding energy contributions to the total affinity (ΔG_{bind}) with the corresponding values (kcal/mol) under co-exposure conditions with graphene nanostructures pristine-Gr and oxidized-Gr. On the lower right side,* ***C)*** *Graphical representation based on per atom-energy contribution for each n-butylbenzene-atom under co-exposure conditions with graphene nanostructures. For this instance, the n-butylbenzene-atoms with the best contribution to the total affinity (ΔG_{bind}) are highlighted (dotted arrows labeled dark-blue) that fit with the light-blue bar for hydrophobic C-atom (C#9, C#10, C#12, and C#15). Herein, the symbol (#) x-axis it was used just for atom-labeling position purposes in the n-butylbenzene structure.*

The simulated co-exposure ***system II***: n-butylbenzene + pristine-Gr + oxidized-Gr show that the most dominant energy contributions for the total affinity (ΔG_{bind}) = -5.90 kcal/mol were provided from non-covalent hydrophobic Van der Waals interactions ΔG_{vdW} > Gauss2 attractive energy contributions. In this regard, the most relevant interacting atoms were the C-atom-labeling positions (C#9, C#10, C#12,

and C#15) which provided the strongest hydrophobic interactions and London non-electrostatic attractive energy contributions. [54,56-59] Likewise, we note that the n-butylbenzene total affinity by the metabolizing TodX-protein significantly decreases in co-exposure conditions and high concentration of graphene nanostructures (pristine-Gr and oxidized-Gr) compared with the affinity reference value-based low-concentration of the n-butylbenzene/TodX complex with ΔG_{bind} = -27.004 kcal/mol (refer to **Figure 3B**). Next, following the same criteria, the third ***system III*** like n-octane + pristine-Gr + oxidized-Gr was evaluated. See **Figure 9**.

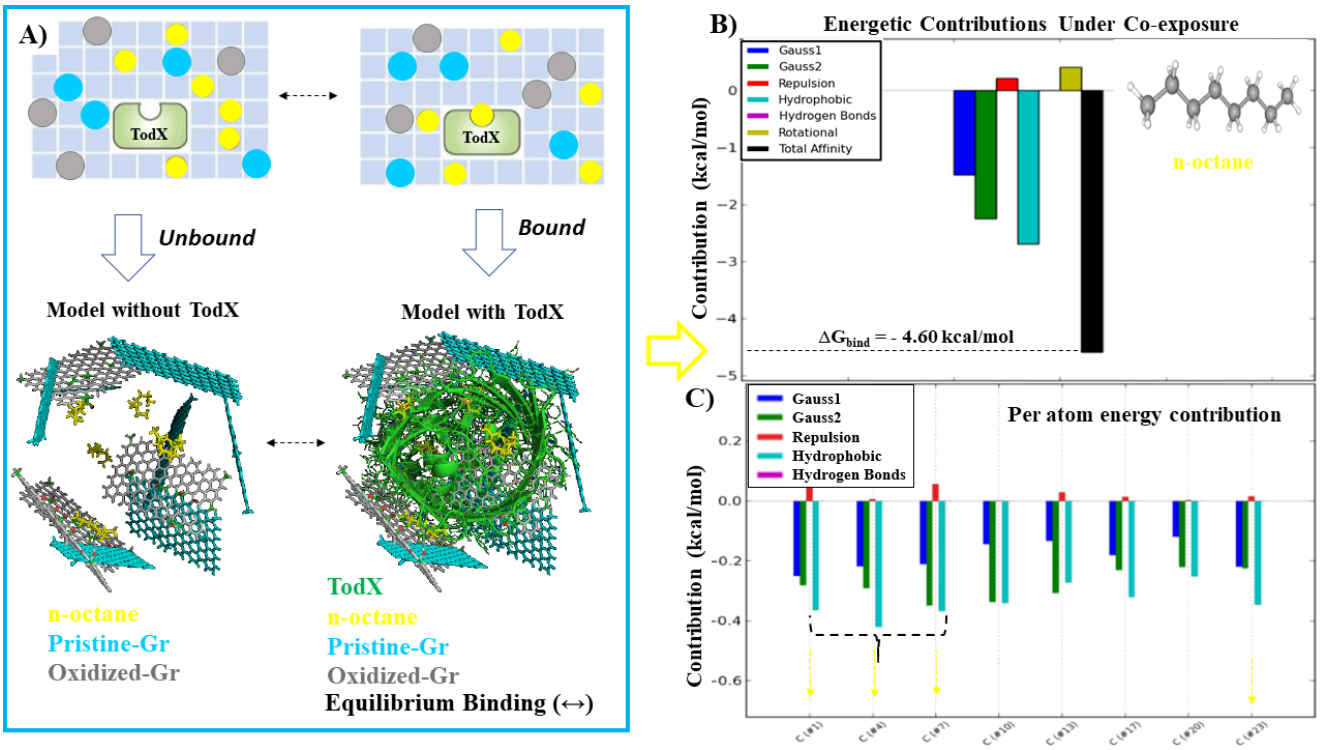

Figure 9. *On the left side,* ***A)*** *Representation of the equilibrium binding-based on the heterogeneous multicomponent docking complex for the* ***system III****: n-octane (yellow) + pristine-Gr (light blue) + oxidized-Gr (gray) in a high concentration of these ligands. Two co-exposure conditions are represented-like: i) without detoxifying TodX protein and ii) with detoxifying TodX protein. On the upper right side,* ***B)*** *Graphical breakdown of the n-octane binding energy contributions to the total affinity (ΔG_{bind}) with the corresponding values (kcal/mol) under co-exposure conditions with graphene nanostructures pristine-Gr and oxidized-Gr. On the lower right side,* ***C)*** *Graphical representation based on per atom-energy contribution for each n-octane-atom under co-exposure conditions with graphene nanostructures. For this instance, the n-octane-atoms with the best contribution to the total affinity (ΔG_{bind}) are highlighted (dotted arrows labeled yellow) that fit with the light-blue bar for hydrophobic C-atom (C#1, C#4, C#7 and C#23). Herein, the symbol (#) x-axis it was used just for atom-labeling position purposes in the n-octane structure.*

In this concern, the total affinity (ΔG_{bind}) = - 4.5 kcal/mol obtained from the n-octane/TodX complex in co-exposure conditions with graphene nanostructures, kept the same pattern on relevant energy

contributions like (ΔG_{vdW} > Gauss2). For this instance, the atoms with the maximum influence in the hydrophobic interactions were the C-atom-labeling positions (C#1, C#4, C#7 and C#23) associated to a significant loss of the relative affinity compared with the simulated condition-based low-concentration with ΔG_{bind} = -24.2392 kcal/mol (refer to **Figure 3C**).

In general terms, as expected the non-covalent hydrophobic interactions leading the main contributions to the total binding affinity with a spontaneous thermodynamic process ($\Delta G_{bind} < 0$) of the three evaluated oil-derived hydrocarbons multicomponent docking systems (*I*, *II*, and *III*) in co-exposure conditions with graphene nanostructures (pristine-Gr and oxidized-Gr) by their chemical properties. [54,56-59] This fact, can be corroborate by the total absence of H-bond interactions with the TodX-protein for the three oil-derived hydrocarbons and, considering the influence of the graphene nanostructures evaluated, which present a well-known network of sp^2-C-atoms with high surface reactivity, which significantly contribute to weaken the affinity of the oil-derived hydrocarbons forming multicomponent docking systems (*I*, *II*, and *III*). In addition, we show that most of the interactions are based on hydrophobic (N···C···C)-backbone and side chain interactions with the catalytic residues from the TodX (site 1).

Then, to briefly show the mutual influence of each ligands composing the heterogeneous multicomponent docking complex in the binding equilibria (unbound and bond) all the energetic contributions under co-exposure conditions are depicted. See **Figure 10**.

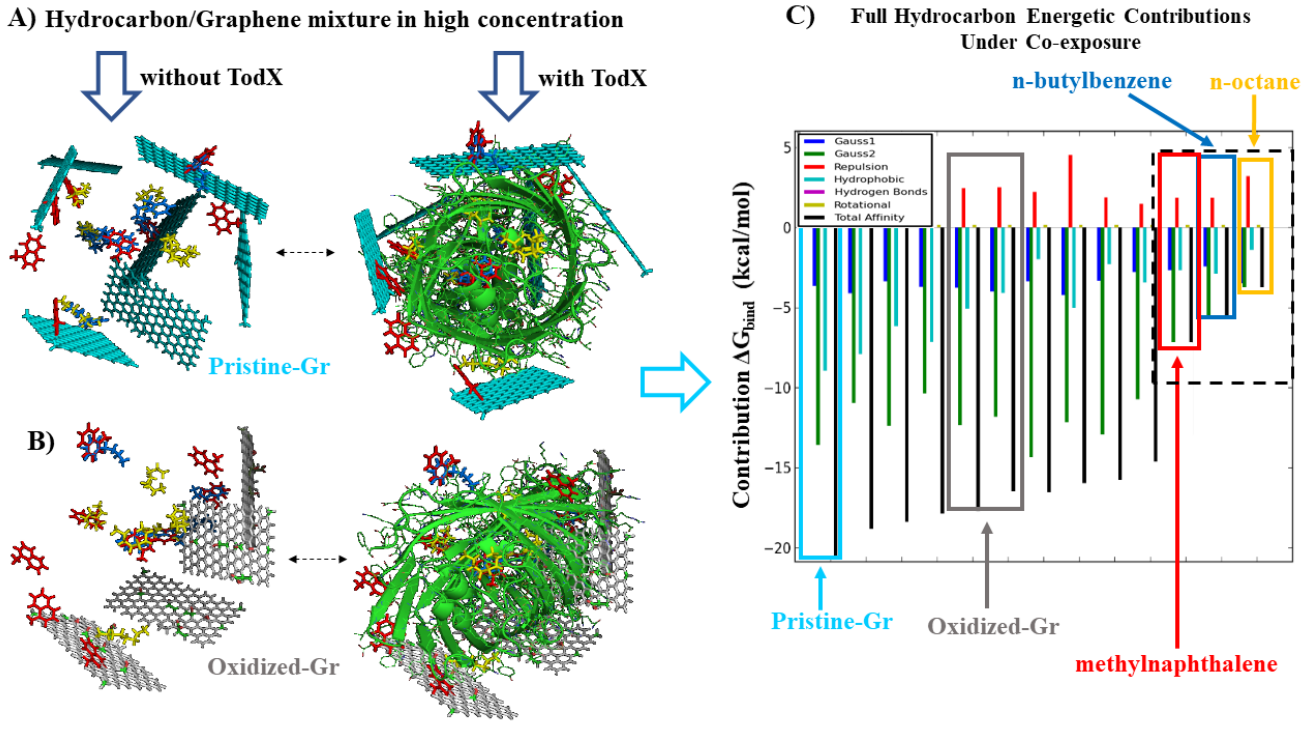

Figure 10. *On the left side,* ***A)*** *Representation equilibrium binding-based Boltzmann model of the heterogeneous multicomponent docking complexes composed by the mixture of all the hydrocarbons interacting with pristine-Gr in the absence and presence of TodX.* ***B)*** *Heterogeneous multicomponent docking complexes composed by the mixture of all the hydrocarbons interacting with oxidized-Gr in the absence and presence of TodX.* ***C)*** *Graphical representation of all the energetic contributions to the*

total affinity (ΔG_{bind}) for each evaluated ligand in co-exposure conditions. Herein, the corresponding values of energetic contributions obtained for the mixture of all the oil-derived hydrocarbons are represented inside the black-dotted line rectangle like: methylnaphthalene (red), n-butyl benzene (blue), n-octane (yellow) and the graphene nanostructures like pristine-Gr (light blue) and oxidized-Gr (gray).

For this instance, is easy to note that in co-exposure conditions with multiple ligands the total affinity-based-binding free energy significantly decrease in all the docking systems following the order: pristine-Gr/TodX > oxidized-Gr/TodX > methylnaphthalene/TodX > n-butylbenzene/TodX > n-octane/TodX maybe because the graphene nanostructures could interact with oil-derived hydrocarbon resulting in a greater amount of TodX protein molecules are in an unbound state (*i.e.,* with unoccupied catalytic sites).[33,34, 54,56-59] On the other hand, the energetic contributions for the total affinity based on repulsive and rotational forces showed a similar behavior for the three oil-derived hydrocarbons/TodX complexes evaluated from the quantitative point of view. Besides, were considered as irrelevant for the stabilization of the multicomponent docking systems (*I*, *II*, and *III*) obtained under co-exposure conditions.[33,34, 54,56-59] These theoretical evidences fit with previous experimental results, which refer that carbon nanomaterials-like graphene's can mitigate the negative environmental impact of many organic compounds interact under co-exposure[15] in a given environmental compartment (water, soil). In this sense, we strongly support hypothesis that the presence of graphene nanostructure significantly reduces the affinity of the oil-derived hydrocarbons limiting its complete detoxification in the TodX-protein, and in this way, increasing its toxicological potential in environmental compartments unless remain adsorbed in the reactive surface of the graphene nanostructures.[15]

To verify the presence of physical-chemical adsorption processes from the graphene nanostructures (pristine-Gr and oxidized-Gr) interacting with the oil-derived hydrocarbons, a DFT study was carried out.[41-44] For this purpose, the electronic and structural properties of the interacting systems, previously defined on the experiment groups (**Group #1**: and **Group #2**), were analyzed and the main results are presented in the **Table 1**.

Table 1. DFT results of graphene nanostructures interacting with oil-derived hydrocarbons, where E_b, d, and **Δ**Q represent the binding energy, minimum distance, and charge transfer, respectively. Herein, the most stable configuration was obtained considering the stability of the formed complexes and denoted by the asterisk (*).

DFT-Group	Ranking	DFT-interacting system	E_b (eV)	d(Å)	**Δ**Q (e^-)
#1	1	pristine-Gr + methylnaphthalene *	- 0.74	2.76	+ 0.05
#1	2	pristine-Gr + n-butylbenzene	- 0.39	3.44	+ 0.22
#1	3	pristine-Gr + n-octane	- 0.66	2.61	+ 0.51
#2	1	oxidized-Gr + methylnaphthalene *	-0.59	2.70	+ 0.06

#2	2	oxidized-Gr + n-octane	-0.44	2.18	+0.08
#2	3	oxidized-Gr + n-butylbenzene	-0.30	2.33	0.00

According to the obtained results, the binding energies (E_b) vary from -0.74 to -0.30 eV characterizing a spontaneous thermodynamic process in all the cases for both groups (Group #1 and Group #2). This fact has a paramount importance, because suggest high probability (*i.e.,* occurrence-based frequency) of interactions and binding affinity for the formed complexes. In the case of the oil-derived hydrocarbons interacting with pristine-Gr (Group #1), the best-ranked binding configuration (*) was found by the pristine-Gr + methylnaphthalene, which presents the highest modular binding-energy value and thermodynamic stability of $| E_b |$ = 0.74 eV with an minimum distance of 2.76 Å. See the **Figure 11**.

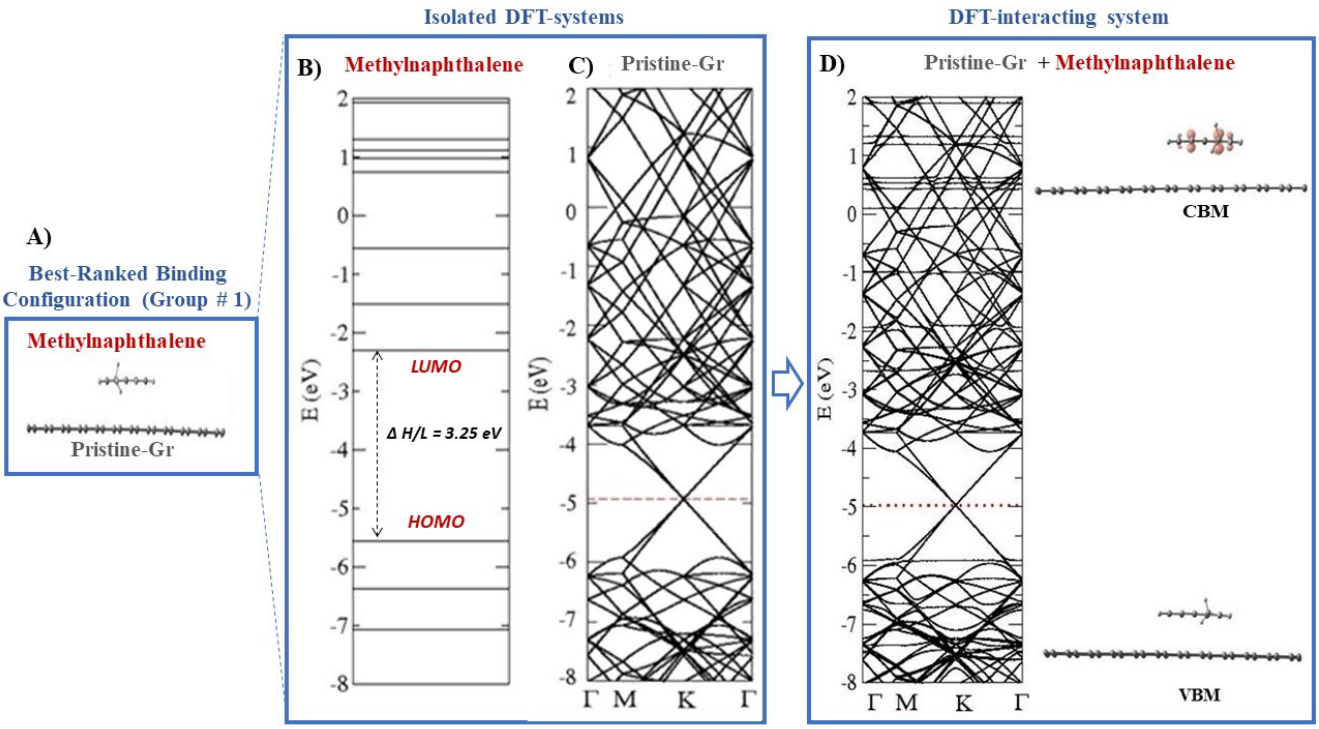

Figure 11. *On the rightmost rectangle,* ***A)*** *Representation of the optimized structures of pristine-Gr (labeled-color gray) and methylnaphthalene (labeled-color red) from the best-ranked binding configuration in the Group #1. In the middle rectangle, are depicted the HOMO/LUMO energy levels and the electronic band structure for the isolated ligands:* ***B)*** *methylnaphthalene molecule (labeled-color red) and* ***C)*** *pristine-Gr (labeled-color gray), respectively. On the leftmost rectangle,* ***D)*** *represents the electronic band structure obtained from the DFT-interacting system formed by pristine-Gr + methylnaphthalene with its corresponding electronic charge density plot. An isosurface value of 0.00096 $e^-/Bohr^3$ was used to represents the charge density associated to conduction band minimum (CBM) and the valence band maximum (VBM). The atom-color labels were represented like: hydrogen-atoms (light-gray) and the carbon-atoms (dark-gray).*

As can be seen from Figure 11A, the methylnaphthalene molecule adopts a parallel position with respect to the pristine-Gr with a value of charge transfer of + 0.05e-, showing that the electron transference

occurs from the pristine-Gr to methylnaphthalene. According to this evidence, we can suggest the presence of a physical adsorption process, without significant modifications on the electronic band structure, around the Fermi region, after the pristine-Gr + methylnaphthalene interaction. Following this idea, we can observe that, in the DFT-interacting system formed by pristine-Gr + methylnaphthalene exists a superposition (Figure 11 D) of the energy levels of the methylnaphthalene molecule (Figure 11 B) with the electronic band structure of the pristine-Gr (Figure 11 C), confirming that the interaction occurs through a physical adsorption regime. Also, the electronic charge density associated to CBM is only concentrated in the methylnaphthalene molecule (Figure 11 D). Further, for this particular isosurface value, no charge concentration was observed in the VBM (Figure 11D), which remain unperturbed for both ligands (methylnaphthalene and pristine-Gr) according to with the calculated binding energy (Eb = - 0.74 eV).

Regarding the main objective of this theoretical study the physical adsorption in the reactive surface of the pristine-Gr is a favorable characteristic toward potential applications as bioremediation strategies and environmental modeling of complexes mixtures.15 Because, it is well-known that the systems which adsorb through weak interaction patterns may present a reversible character during the complex formation, which allows the easy removal of the desired compounds (as oil-derived hydrocarbons) from the environmental compartments (water, soil), and later, the system could be efficiently reused in subsequent treatments, in the case of this nanostructure (pristine-Gr).15,60

By the other hand, the system formed by the oxidized-Gr + methylnaphthalene DFT-results were also identified like the best-ranked binding configuration (*) in the DFT-Group #2 with the highest modular binding-energy value and thermodynamic stability | Eb | = 0.59 eV compared with the other two DFT-complexes like oxidized-Gr + n-octane (| Eb | = 0.44 eV) and oxidized-Gr + n-butylbenzene (| Eb | = 0.30 eV). For this most stable configuration, the obtained value for the charge transfer, between an H-atom from the methylnaphthalene with an O-atom from oxidized-Gr, was + 0.06 e-. The electronic characteristics of the oxidized-Gr + methylnaphthalene system are shown in the Figure 12.

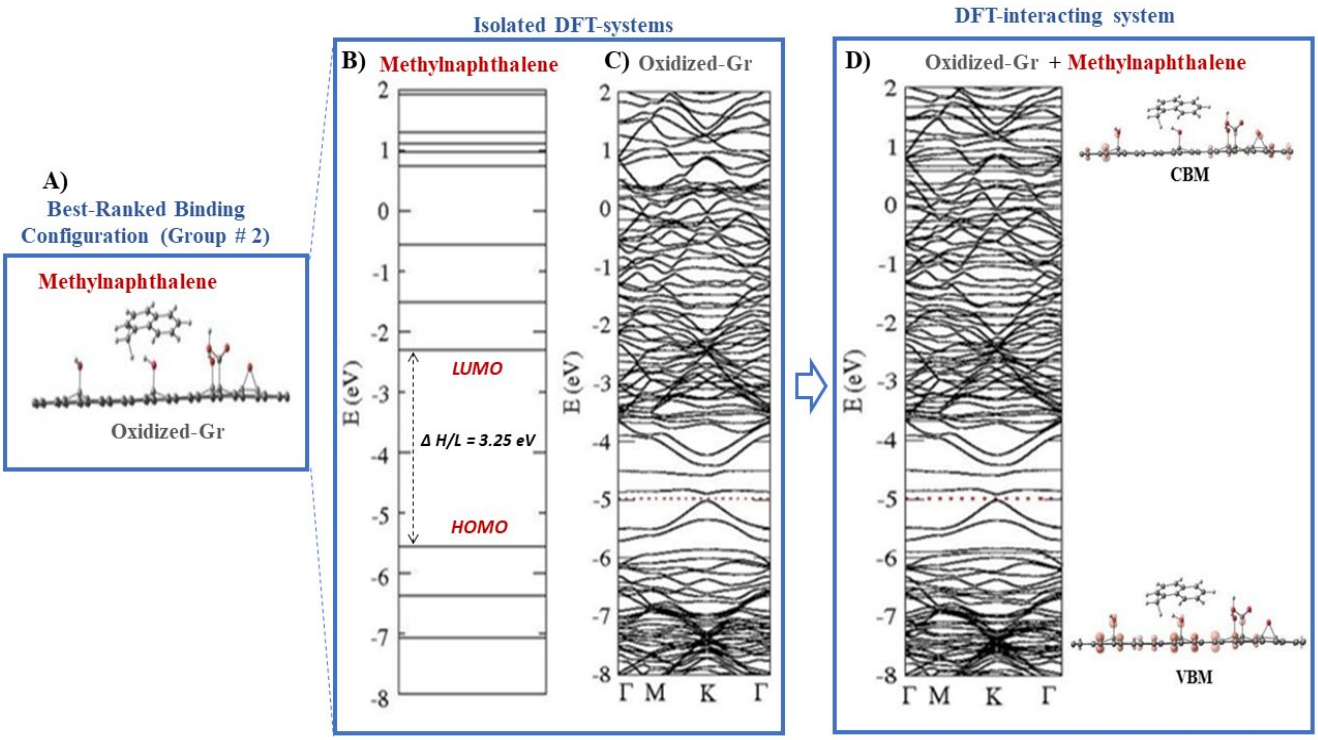

Figure 12. *On the rightmost rectangle,* ***A)*** *Representation of the optimized structures of oxidized-Gr (labeled-color gray) and methylnaphthalene (labeled-color red) from the best-ranked binding configuration in the Group #2. In the middle rectangle, are depicted the HOMO/LUMO energy levels and the electronic band structure for the isolated ligands:* ***B)*** *methylnaphthalene (labeled-color red) molecule and* ***C)*** *oxidized-Gr (labeled-color gray), respectively. On the leftmost rectangle,* ***D)*** *represents the electronic band structure obtained from the DFT-interacting system formed by oxidized-Gr + methylnaphthalene with its corresponding electronic charge density plot. An isosurface value of 0.00096 $e^-/Bohr^3$ was used to represents the charge density associated to conduction band minimum (CBM) and the valence band maximum (VBM). The atom-color labels were represented like: oxygen-atoms (red), hydrogen-atoms (light-gray), and the carbon-atoms (dark-gray).*

Herein, no significant differences were observed between the electronic properties of the isolated oxidized-Gr system (**Figure 12 C**), with respect to the oxidized-Gr + methylnaphthalene system (**Figure 12 D**). We note the presence of superposition of the energy levels of the methylnaphthalene molecule (**Figure 12 B**) with the electronic band structure of the oxidized-Gr after the interaction (**Figure 12 D**), suggesting that the interaction occurs also through a physical adsorption regime in the **DFT-Group #2,** similar to the most stable system in the **DFT-Group #1**. As a difference, it is important to highlight that, in the case of the oxidized-Gr + methylnaphthalene system, the results of electronic charge density plot show that the charges were only concentrated on the oxidized-Gr nanostructure in both CBM and VBM edges (**Figure 12 D**).

In this context, the current results suggest that the pristine-Gr has a higher capacity to bind hydrophobic molecules like oil-derived hydrocarbon as compared with the oxidized-Gr, due to the π - π interactions

between the graphene atoms and the aromatic rings of the adsorbed molecules. In addition, these theoretical evidences have been experimentally observed in previous works performed by Wang et al. (2014),[12] in which they show that the interaction affinity between hydrocarbons and carbon nanostructures are favored by the physical adsorption mechanism-based on hydrophobic π- π interactions between the sp^2-C atoms from aromatic rings of the molecules.[15,60]

An overview of our theoretical results strongly suggests that environmental mixtures of oil-derived hydrocarbon with carbon nanomaterials like graphene can potentially reduce the ecotoxicological impact of many other pollutants of high persistence in the environment. In this sense, the theoretically evaluated adsorption mechanism mimicking a well-recognized *Trojan-horse phenomenon* which leading most of the interaction processes for engineered organic nanomaterials (NM).[15,60] Nevertheless, still a long way to explore, since the physico-chemical mechanisms in the nanoscale, exhibit nonlinear behaviors (*i.e.,* nonlinear concentration-response relationships in the environmental compartments like water, soil and air), which depend on the global physical and chemical properties of a given mixture and the biological model used (molecules, proteins, cells, organism, ecosystems).

Conclusions

In the present study, we tackle the environmental modeling on the co-exposure of a heterogeneous complex mixture of oil-derived hydrocarbons, mimicking high concentrations in the presence of the detoxifying protein from *Pseudomonas putida* (TodX) and graphene nanostructures. For the first time, new mechanistic approaches-based on molecular docking and DFT-simulations were performed in order to explore the interactions of hydrocarbons that present a high environmental impact. The results on structural modeling-based Ramachandran structural validation revealed that the TodX protein can be efficiently modeled with a crystallographic quality (> 70%) with absence of flexibility restrictions for the ligand-binding residues, which are involved in the transport and biodegradation of complex mixtures of oil-derived hydrocarbon.

The obtained results performing a flexible docking simulation coupled to 3D-lig-plot diagrams allowed mimicking relevant interactions of the oil-derived hydrocarbon (methylnaphthalene, n-butylbenzene, and n-octane) in low-concentrations of the oil-derived hydrocarbons. For this instance, the Gibbs free energy of binding of the formed complexes (oil-derived hydrocarbon + TodX) exhibit a spontaneous thermodynamic processes ($\Delta G_{bind} < 0$ kcal/mol), with prevalence of non-covalent hydrophobic interactions in the TodX-binding site 1 from with an obtained average FEB-values around ≈ - 25.35 kcal/mol from the three hydrocarbon.

On the other hand, the graphene nanostructures interact in a different biophysical environment (TodX-binding site 2); describing spontaneous thermodynamic processes following the order FEB (TodX/pristine-Gr complex) = - 26.332 kcal/mol > FEB (TodX/oxidized-Gr complex) = -20.132 kcal/mol according to the strength of the interactions. In addition, the graphene interactions in the TodX-

binding site 2 can modulate the responses on the TodX-binding site 1, affecting the communication efficiency in the ToDX residue-network. Besides, the modeling results using heterogeneous multicomponent docking approach (oil-derived hydrocarbons + graphene nanostructures + TodX protein) and DFT-simulation, show a significant decrease of the total affinity of the oil-derived hydrocarbons by the TodX (site 1) with an obtained average FEB-values around ≈ - 5.8 kcal/mol compared with the affinity of the complex mimicking low-concentrations FEB-values (oil-derived hydrocarbon + TodX) = - 25.35 kcal/mol from the three hydrocarbons. According to this, the general DFT-results suggest the occurrence of physical adsorption mechanism in the reactive surface of the graphene nanostructures (pristine-Gr > oxidized-Gr), mimicking a *Trojan-horse phenomenon*, which is well-recognized leading the most interactions for organic nanomaterials under co-exposure with complex mixtures.

Finally, these theoretical results open new horizons to improve bioremediation strategies to prevent the negative impact of multiple oil-derived hydrocarbons under environmental co-exposure and to ensure a safe and sustainable use of the graphene nanomaterials-based nanotechnologies applications.

Corresponding Authors

*Fax: 55-32226484. Email: patiolivera@yahoo.com.br,
*Fax: +351220402659. Email: michael.durruthy@fc.up.pt,
*Fax: 55-32226484. Email: solange.fagan@gmail.com,

ORCID

Patricia Viera de Oliveira: 0000-0003-2587-3855

Michael González-Durruthy: 0000-0002-7061-0811

Disclosure statement

The authors declare no competing interests.

Ackowledgments

This work received financial support from Fundação para a Ciência e a Tecnologia (FCT/MEC). The work of M. G.-D. and M. N. D. S. Cordeiro was supported by UID/QUI/50006/2019 with funding from FCT/MCTES through national funds. J.M.R acknowledge Xunta de Galicia (ED431B 2017/21, ED41E2018/08). Also, the authors acknowledge the financial support from the Coordenação de Aperfeiçoamento de Pessoal de Nível Superior - Brasil (CAPES), CNPq, and the Centro Nacional de Processamento de Alto Desempenho (CENAPAD) for the computational time.

References

1. Barron, M. G. Ecological impacts of the Deepwater Horizon oil spill: implications for immunotoxicity. *Toxicol. Pathol*, **2012**, 40, 315-320.

2. Goldstein, B. D., Osofsky, H. J., & Lichtveld, M. Y. The Gulf oil spill. *New Eng. Journ. Med.* **2011**, 364, 1334-1348.
3. Beyer, J., Trannum, H. C., Bakke, T., Hodson, P. V., & Collier, T. K. (2016). Environmental effects of the Deepwater Horizon oil spill: a review. *Marine pollution bulletin*. **2016**, 110, 28-51.
4. Balba, M. T., Al-Awadhi, N., & Al-Daher, R. Bioremediation of oil-contaminated soil: microbiological methods for feasibility assessment and field evaluation. *Journ. Microbiol Meth*. **1998**, 32, 155-164.
5. Adams, G. O., Fufeyin, P. T., Okoro, S. E., & Ehinomen, I. Bioremediation, biostimulation and bioaugmention: a review. *Inter. Journ. Environm. Bioremed & Biod*, **2015**, 3, 28-39.
6. Raghavan, P. U. M., & Vivekanandan, M. Bioremediation of oil-spilled sites through seeding of naturally adapted Pseudomonas putida. *Intern biodeterioration & biodegradation*, **1999**, 44, 29-32.
7. Nwachukwu, S. C., James, P., & Gurney, T. R. Inorganic nutrient utilization by "adapted" Pseudomonas putida strain used in the bioremediation of agricultural soil polluted with crude petroleum. *Journ. Environm. Biology*, **2001**, 22, 153-162.
8. Belchik. A β-barrel outer membrane protein facilitates cellular uptake of polychlorophenols in *Cupriavidus necator*. *Biodegradation*. **2010**, 21, 431-439.
9. Van den Berg, B. Going forward laterally: transmembrane passage of hydrophobic molecules through protein channel walls. *Chembiochem*, **2010**, *11*, 1339-1343.
10. Mardani, G., Mahvi, A. H., Hashemzadeh-Chaleshtori, M., Naseri, S., Dehghani, M. H., & Ghasemi-Dehkordi, P. Application of Genetically Engineered Dioxygenase Producing *Pseudomonas putida* on Decomposition of Oil from Spiked Soil. *Jundishapur Journ. Nat. Pharm. Prod.* **2017**, *12* (3 (Supp)).
11. Kharisov, B. I., Dias, H. R., & Kharissova, O. V. Nanotechnology-based remediation of petroleum impurities from water. *Journ. Petrol. Sci. Eng.* **2014**, 122, 705-718.
12. Wang, J., Chen, Z., & Chen, B. Adsorption of polycyclic aromatic hydrocarbons by graphene and graphene oxide nanosheets. *Environm. Sci. Technol.* **2014**, 48, 4817-4825.
13. Iqbal, M. Z., & Abdala, A. A. Oil spill cleanup using graphene. *Environm. Sci. Poll. Res.* **2013**, 20, 3271-3279.
14. Robbins, W. K., & Hsu, C. S. Petroleum, Composition. *Kirk-Othmer Encyclopedia of Chemical Technology.* **2000**.
15. Naasz, S., Altenburger, R., Dana Kühne. Environmental mixtures of nanomaterials and chemicals: The *Trojan-horse* phenomenon and its relevance for ecotoxicity. *Journ. Sci. Tot. Env.* 2018, 635, 1170-1181.
16. Xu, X., Liu, Wenming., Tian, S., Wang, W., Qi, Qige., Jiang, Pan., Gao, Xinmei., Li, Fengjiao., Li, Haiyan., Yu, Hongwen. Petroleum Hydrocarbon-Degrading Bacteria for the Remediation of Oil Pollution Under Aerobic Conditions: A Perspective Analysis. *Front. Microbiol*. **2018**, 9, 2885.
17. Adebajo, M.O., Frost, R.L., Kloprogge, J.T., Carmody, O., Kokot, S. Porous materials for oil spill cleanup: a review of synthesis and absorbing properties. *J. Porous Mater*. **2003**, 10 , 159-170.
18. Martín de Lucía, I., Campos-Mañas, M.C., Agüera, A., Rodea-Palomares, I., G., Francisco Leganés, Fernández-Piñas, F., and Rosa, R. Reverse Trojan-horse effect decreased wastewater toxicity in the presence of inorganic nanoparticles. ***Environ. Sci.: Nano***. 2017,**4**, 1273-1282.
19. Lun Hsiao, I., Kong Hsieh, Yi., Chu-Fang W., Chieh, Chen., Yuh-Jeen, Huang. Trojan-Horse Mechanism in the Cellular Uptake of Silver Nanoparticles Verified by Direct Intra- and Extracellular Silver Speciation Analysis. *Environ. Sci. Technol.* 2015, 49, 3813-3821.

20. Jiménez, J., Doerr, S., Martínez-Rosell, G., Rose, A. S., & De Fabritiis, G. DeepSite: protein-binding site predictor using 3D-convolutional neural networks. *Bioinformatics*, **2017**,33, 3036-3042.
21. Feinstein, W. P., & Brylinski, M. Calculating an optimal box size for ligand docking and virtual screening against experimental and predicted binding pockets. *J Cheminform*. **2015**, *7*, 18.
22. Forli, S., Huey, R., Pique, M. E., Sanner, M. F., Goodsell, D. S., & Olson, A. J. (2016). Computational protein–ligand docking and virtual drug screening with the AutoDock suite. *Nat Protoc*, **2016**, 11, 905.
23. Vincent B. Chen, W. Bryan Arendall III, Jeffrey J. Headd, Daniel A. Keedy, Robert M. Immormino, Gary J. Kapral, Laura W. Murray, Jane S. Richardson and David C. Richardson. MolProbity: all-atom structure validation for macromolecular crystallography. *Acta Crystallographica*. **2010**, 66: 12-21.
24. Mitternacht, S., Berezovsky, I.N. Coherent Conformational Degrees of Freedom as a Structural Basis for Allosteric Communication. *Plos. Comput. Biol.* ***2011,*** 7, e1002301.
25. Ozlem Keskin, Stewart R. Durell, Ivet Bahar, Robert L. Jernigan, and David G. Covell. Relating Molecular Flexibility to Function: A Case Study of Tubulin. *Biophys Journ*. **2002**, 83, 663–680.
26. Greener, J.G., Sternberg, M.J.E. AlloPred: prediction of allosteric pockets on proteins using normal mode perturbation analysis. *BMC Bioinformatics*. **2015**, 16, 335.
27. Hearn, E.M., Patel, D.R., Bert van den Berg. Outer-membrane transport of aromatic hydrocarbons as a first step in biodegradation. *PNAS*, **2008**, 105, 8601-8606.
28. Trott, O., & Olson, A. J. AutoDock Vina: improving the speed and accuracy of docking with a new scoring function, efficient optimization, and multithreading. *J Comput Chem*, **2010**, 31, 455-461.
29. Morris, G. M., Goodsell, D. S., Halliday, R. S., Huey, R., Hart, W. E., Belew, R. K., & Olson, A. J. Automated docking using a Lamarckian genetic algorithm and an empirical binding free energy function. *J Comput Chem*. **1998**, *19*, 1639-1662.
30. Berman, H. M., Westbrook, J., Feng, Z., Gilliland, G., Bhat, T. N., Weissig, H., Shindyalov, I. N., and Bourne, P. E. The Protein Data Bank. *Nucleic Acids Res.* **2000***, 28*, 235-242.
31. Xie, Z. R., & Hwang, M. J. An interaction-motif-based scoring function for protein-ligand docking. *BMC bioinformatics*, **2010**, 11, 298.
32. Kim, S., Thiessen, P.A., Bolton, E.E., Chen, J., Fu, G., Gindulyte, A., Han, L., He, J., He, S., Shoemaker, B.A., Wang, J., Yu, B., Zhang, J., Bryant, S.H. PubChem substance and compound databases. *Nucleic Acids Res*. **2016**, 44, 202–1213.
33. Feldman H.A. Mathematical Theory of Complex Ligand-Binding Systems at Equilibrium: Some Methods for Parameter Fitting. *Anal. Biochem*. **1972**, 48, 317-338.
34. Haiech, J, Gendrault, Y., Kilhoffer, M.C., Ranjeva, R., Madec, M., Lallement, C. A general framework improving teaching ligand binding to a macromolecule. *Bioch. Biophys. Act*. 2014, 1843, 2348–2355.
35. Seeliger, D., & de Groot, B. L. Ligand docking and binding site analysis with PyMOL and Autodock/Vina., *J Comput Aided Mol Des.* ***2010,*** *24*, 417-422.
36. Laskowski, R.A, Swindells, M.B. LigPlot+: Multiple LigandProtein Interaction Diagrams for Drug Discovery. *J. Chem. Inf. Model*. **2011**, 51, 2778–2786.
37. Aoxiang Tao, Dong Xu, et al. ezCADD: A Rapid 2D/3D Visualization-Enabled Web Modeling Environment for Democratizing Computer-Aided Drug Design. : *J. Chem. Inf. Model*. **2019**, 59, 18−24.
38. da Silveira, C. H., Pires, D. E., Minardi, R. C., Ribeiro, C., Veloso, C. J., Lopes, J. C., Santoro, M. M. Protein cutoff scanning: A comparative analysis of cutoff dependent and cutoff free methods for prospecting contacts in proteins. *Proteins: Struct Funct Bioinf.* **2009**, 74, 727-743.

39. Rarey, M., Kramer, B., & Lengauer, T. Multiple automatic base selection: Protein–ligand docking based on incremental construction without manual intervention. *J Comput Aided Mol Des*, **1997**, *11*: 369-384.
40. Shoichet, B. K. Virtual screening of chemical libraries. *Nature.* **2004***,* 432, 862-865.
41. Soler, J. M., Artacho, E., Gale, J. D., García, A., Junquera, J., Ordejón, P., & Sánchez-Portal, D. The SIESTA method for ab initio order-N materials simulation. *J. Phys. Condens. Matter*. **2002**, 14, 2745.
42. Kohn, W., & Sham, L. J. Self-consistent equations including exchange and correlation effects. *Phys. Rev*.**1965**, 140, 1133.
43. Perdew, J. P., & Zunger, A. Self-interaction correction to density-functional approximations for many-electron systems. *Phys. Rev. B*. **1981**, 23, 5048.
44. Troullier, N., & Martins, J. L. Efficient pseudopotentials for plane-wave calculations. *Phys. Rev. B*, **1991**, 43, 1993.
45. Adipah, S. Introduction of Petroleum Hydrocarbons Contaminants and its Human Effects. *Journ. Env. Sci. Pub. Health.* **2019**, 3, 001-009.
46. Das, N., Chandran, P. Microbial Degradation of Petroleum Hydrocarbon Contaminants: An Overview. *Biotechnol. Res. Inter*. **2010**, 10, 1-13.
47. Gray, J. S. Biomagnification in marine systems: the perspective of an ecologist. *Mar Pollut Bull*. 2002, 45, 46-52.
48. Riisgaard, H.U., Hansen, S. Biomagnification of mercury in a marine grazing food-chain: algal cells *Phaeodactylum tricornutum*, mussels *Mytilus edulis* and flounders *Platichthys flesus*studied by means of a stepwise-reduction-CVAA method. *Mar. Ecol. Prog. Ser*. **1990**, 62, 259-270.
49. Strandberg, B., Bandh, C., Van Bavel B., Bergqvist P. A. , Broman, D., Naef, C., Pettersen, H., Rappe, C. Concentrations, biomagnification and spatial variation of organochlorine compounds in a pelagic food web in the northern part of the Baltic Sea. *Sci. Total Environ*. **1998**, 217, 143-154.
50. Ikeda, K.; Hirokawa, T.; Higo, J.; Tomii, K., Protein-segment universe exhibiting transitions at intermediate segment length in conformational subspaces. *BMC. Struct Biol* **2008,** *8*.
51. Patlewicz, G., Worth, A. P., and Ball, N. Validation of Computational Methods. *Adv Exp Med Biol*. 2016, *856*, 165-187.
52. OECD Principles for the validation, for regulatory purposes of (Quantitative) Structure Activity Relationship Model. http: www.oecd.org/(accessed 26/08/**2019**).
53. ISO/TC 229 Nanotech., **2011**.
54. Benko, H. ISO Technical Committee 229 Nanotechnologies. Metrology and Standardization of Nanotechnology: Protocols and Industrial Innovations. **2017,** 527-34039.
55. Ghosh, S., Ojha, P. K, Roy, K. Exploring QSPR modeling for adsorption of hazardous synthetic organic chemicals (SOCs) by SWCNTs. *Chemosphere*, **2019**, 228, 545-555.
56. Haiech, J., Vallet, B., Aquaron, R., Demaille, J.G. Ligand binding to macromolecules: determination of binding parameters by combined use of ligand buffers and flow dialysis; application to calcium-binding proteins, *Anal. Biochem.* **1980**,105, 18–23.
57. J.E. Fletcher, J.E., Spector, A.A., Ashbrook, J.D. Analysis of macromolecule—ligand binding by determination of stepwise equilibrium constants, *Biochem*. **1970**, 9, 4580–4587.
58. Klotz, I.M., Hunston, D.L. Mathematical models for ligand–receptor binding. Real sites, ghost sites, *J. Biol. Chem*. **1984**, 259, 10060-10062.
59. Klotz, I.M. Ligand—receptor interactions: facts and fantasies, *Q. Rev. Biophys.* **1985**, 18, 227—259.
60. Konkoli, Z. Safe uses of Hill's model: an exact comparison with the Adair—Klotz model, *Theor. Biol. Med. Model*. **2011**, 8, 10.
61. Sánchez-Linares, I., Pérez-Sánchez, H., Cecilia, J.M., García, J, M. High-throughput parallel blind virtual screening using BINDSURF. *BMC Bioinformatics*. **2012**, 13, 13.

62. Jauris, I.M., Matos, C. F. , Saucier C., Lima, E. C., Zarbin, A. J. G., Fagan, S. B., Machado, F. M. , Zanella, I. Adsorption of sodium diclofenac on graphene: a combined experimental and theoretical study. *Phys. Chem. Chem. Phys*. **2016,** 18, 1526-1536.